

RESEARCH ARTICLE SUMMARY

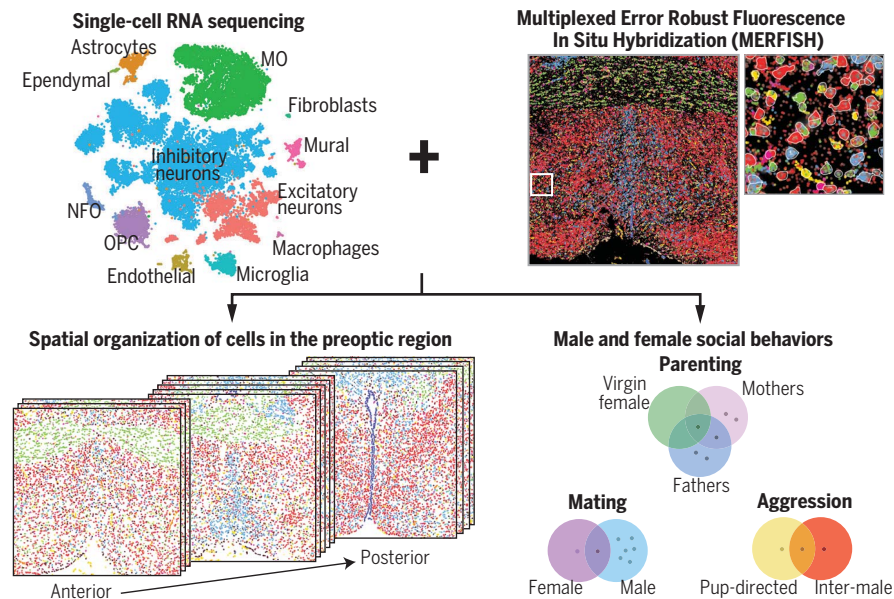
NEUROGENOMICS

Molecular, spatial, and functional single-cell profiling of the hypothalamic preoptic region

Jeffrey R. Moffitt*, Dhananjay Bambah-Mukku*, Stephen W. Eichhorn†, Eric Vaughn†, Karthik Shekhar, Julio D. Perez, Nimrod D. Rubinstein, Junjie Hao, Aviv Regev, Catherine Dulac‡§, Xiaowei Zhuang‡§

INTRODUCTION: A mechanistic understanding of brain function requires the identification of distinct cell types in the brain at a molecular, spatial, and functional level. The preoptic region of the hypothalamus comprises multiple nuclei and controls many social behaviors and homeostatic functions. Discrete neuronal types within the preoptic region have been associated with specific hypothalamic behaviors and homeostatic controls, yet the organizational principles of the underlying circuits remain elusive. Further progress requires methods that can identify molecularly distinct cell types and map their spatial and functional organization in the tissue.

RATIONALE: Single-cell RNA sequencing (scRNA-seq) has revolutionized the understanding of many tissues by allowing a systematic, genome-wide molecular identification of cell types. However, scRNA-seq requires cell dissociation, leading to a loss of spatial context that is essential to understand the cellular architecture of brain circuits. Image-based approaches to single-cell transcriptomics enables gene expression profiling of individual cells within their native tissue and offers opportunities for simultaneous *in situ* cell-type identification and spatial mapping, as well as functional characterization when combined with activity marker imaging. The combination of these complementary tech-



In situ single-cell profiling reveals the molecular and cellular organization of the hypothalamic preoptic region. The combination of MERFISH with scRNA-seq to profile the gene expression of 1 million cells *in situ* revealed ~70 neuronal populations in the preoptic region, each with distinct molecular signatures and spatial organizations, providing insights into neuromodulatory signaling pathways. Further combination with activity marker imaging led to the identification of discrete neuronal types activated by key social behaviors, including parenting, aggression, and mating.

niques would allow us to generate a molecular inventory of neuronal types while mapping their spatial and functional organization.

RESULTS: We combined scRNA-seq and multiplexed error robust fluorescence *in situ* hybridization (MERFISH), a single-cell transcriptome imaging method, to investigate the molecular, spatial, and functional organization of the mouse hypothalamic preoptic region. We profiled ~31,000 cells using scRNA-seq and imaged ~1.1 million cells within intact tissues using

MERFISH. Our data revealed a remarkable diversity of neurons in this region, comprising ~70 different neuronal populations, many of which were previously unknown. These

neuronal types exhibited distinct neuromodulatory signatures and revealed a striking heterogeneity within cell populations that were previously thought to be functionally unitary. MERFISH measurements further allowed us to map the spatial organization of these neuronal types, determine the cellular composition of distinct nuclei, and provide insights into the functional organization of neuron populations, including topographical relationships that underlie sex hormone signaling.

Last, we combined MERFISH with immediate-early-gene expression imaging to identify specific neuronal populations activated by social behaviors, including parenting, mating, and aggression. Several neuronal populations were selectively activated in each of these behaviors, supporting the notion that transcriptionally distinct neuronal types control specific hypothalamic functions. We identified a core neuronal population activated in all animals that exhibit parenting, as well as cell populations differentially activated in mothers and fathers, providing insights into how physiological state may affect parental behavior. Moreover, we identified cells associated with sexual behavior in males and females as well as male aggression toward infants and conspecific males.

CONCLUSION: By combining MERFISH with scRNA-seq, we have revealed the molecular, spatial, and functional organization of neurons within the hypothalamic preoptic region. These results provide a framework for mechanistic investigation of behavior circuits with high molecular and spatial resolution and opens avenues for identifying and mapping cell types in a diverse range of tissues and organisms. ■

The list of author affiliations is available in the full article online.

*These authors contributed equally to this work.

†These authors contributed equally to this work.

‡These authors contributed equally to this work.

§Corresponding author. Email: dulac@fas.harvard.edu (C.D.); zhuang@chemistry.harvard.edu (X.Z.)

Cite this article as J. R. Moffitt et al., *Science* **362**, eaau5324 (2018). DOI: 10.1126/science.aau5324

RESEARCH ARTICLE

NEUROGENOMICS

Molecular, spatial, and functional single-cell profiling of the hypothalamic preoptic region

Jeffrey R. Moffitt^{1,2,3,4,*}, Dhananjay Bambah-Mukku^{1,4,5*}, Stephen W. Eichhorn^{1,2,3,4,†}, Eric Vaughn^{1,4,5†}, Karthik Shekhar⁶, Julio D. Perez^{1,4,5}, Nimrod D. Rubinstein^{1,4,5}, Junjie Hao^{1,2,3,4}, Aviv Regev^{1,6,7}, Catherine Dulac^{1,4,5,†§}, Xiaowei Zhuang^{1,2,3,4,†§}

The hypothalamus controls essential social behaviors and homeostatic functions. However, the cellular architecture of hypothalamic nuclei—including the molecular identity, spatial organization, and function of distinct cell types—is poorly understood. Here, we developed an imaging-based *in situ* cell-type identification and mapping method and combined it with single-cell RNA-seq to create a molecularly annotated and spatially resolved cell atlas of the mouse hypothalamic preoptic region. We profiled ~1 million cells, identified ~70 neuronal populations characterized by distinct neuromodulatory signatures and spatial organizations, and defined specific neuronal populations activated during social behaviors in male and female mice, providing a high-resolution framework for mechanistic investigation of behavior circuits. The approach described opens a new avenue for the construction of cell atlases in diverse tissues and organisms.

A mechanistic understanding of brain function requires a systematic assessment of cell types and their spatial organization, connectivity, and functional properties. A case in point is the preoptic region of the hypothalamus, which comprises multiple nuclei and controls essential social behaviors such as parenting, mating, and aggression as well as homeostatic functions such as thermoregulation, thirst, and sleep (1, 2). Because these are evolutionarily conserved functions, it has been proposed that the associated neural circuits are genetically defined and thus composed of transcriptionally distinct neuronal types (1–3). Indeed, several neuronal populations within the preoptic region, each defined by discrete molecular markers, have been linked to distinct behavioral and homeostatic functions (4–11). However, the number of cell types present in the preoptic region as well as their molecular signatures, spatial organizations, and functional roles remain unclear, hampering our ability to investigate the underlying neural circuits.

Single-cell RNA-seq (scRNA-seq) provides a powerful means for the identification of cell types and cell states through genome-wide expression profiling of individual cells, offering rich insights into the cellular diversity of many tissues, including the brain (12–15). However, scRNA-seq requires cell dissociation and thus results in the loss of the spatial context of cells that is critical for understanding tissue function (15, 16). Recently, image-based single-cell transcriptomic approaches have been developed that quantify gene expression by directly imaging individual RNA molecules within intact cells and tissues with multiplexed fluorescence *in situ* hybridization (FISH) or *in situ* sequencing (15, 17–22). These approaches offer new opportunities to identify cell populations within complex tissues while simultaneously mapping their spatial organization and uncovering their functions by combining gene expression profiling with imaging of activity markers, such as the induction of immediate early genes (IEGs) (22, 23). Among these, multiplexed error-robust FISH (MERFISH) detects individual RNA molecules with single-molecule FISH (smFISH) (24, 25) and uses error-robust barcoding, combinatorial labeling, and sequential imaging to multiplex smFISH measurements, enabling transcriptome-scale RNA imaging of individual cells *in situ* (20, 26).

We developed a MERFISH-based imaging and analysis platform for *in situ* cell-type identification and mapping and used this approach, in combination with scRNA-seq, to create a cell atlas of the preoptic region of the mouse hypothalamus. We used scRNA-seq to catalog cell populations and identify their marker genes.

We then performed MERFISH imaging of these marker genes together with genes of known functional importance to identify cell populations and map their spatial organization *in situ*. Last, we combined MERFISH with measurements of IEG expression in order to identify discrete cell populations activated by specific social behaviors—including parenting, aggression, and mating—in both sexes and different physiological states.

Results

scRNA-seq of the preoptic region

We dissected a rostral part of the mouse hypothalamus that contains the preoptic region (Fig. 1A)—the medial preoptic area (MPOA) and surrounding nuclei (~2.5 by 2.5 by 1.1 mm, Bregma +0.5 to -0.6)—from adult female and male brains and dissociated the tissue using a custom protocol that improved cell survival and capture (fig. S1). We collected scRNA-seq profiles from 31,299 cells across three replicates of each sex using droplet-based scRNA-seq (27–29).

We used unsupervised, graph-based, community-detection methods (28, 30, 31) modified by us (fig. S2) to cluster cells (29). This led to the delineation of major cell classes, including inhibitory and excitatory neurons, microglia, astrocytes, immature oligodendrocytes (newly formed oligodendrocytes and oligodendrocyte progenitor cells), mature oligodendrocytes, ependymal cells, endothelial cells, fibroblasts, macrophages, and mural cells, as well as subdivisions within these cell classes (Fig. 1B and table S1).

Further clustering of inhibitory neurons (15,042 cells) and excitatory neurons (3511 cells) separately revealed 43 and 23 subpopulations, respectively (Fig. 1B; fig. S3, A and B; and tables S1 and S2). Hereafter, we denote excitatory and inhibitory neuronal clusters as e1, e2, ..., and i1, i2, ..., respectively. We also provide specific names for these clusters based on marker genes (Fig. 1, C and D, and figs. S4 and S5, the latter emphasizing neuropeptide expression) (29).

Although the majority of the identified clusters expressed either excitatory or inhibitory neuronal markers, we observed expression of the γ -aminobutyric acid (GABA) synthetic genes Gad1 and Gad2 in many excitatory neuronal clusters classified on the basis of expression of Vglut2 (Slc17a6), with Gad2 expression being particularly widespread (fig. S3C). By contrast, very few Slc17a6-positive clusters expressed the GABA transporter gene Vgat (Slc32a1). These data suggest that Slc17a6 and Slc32a1 are better discriminators for excitatory versus inhibitory neurons, corroborating evidence from other brain areas (32). Cells in two neuronal clusters originally designated as inhibitory and one originally designated as excitatory coexpressed Slc17a6 (or Slc17a8, vGlut3) and Slc32a1. These cells were unlikely to be a clustering artifact because individual cells coexpressed both markers, nor did they correspond to doublets (29); hence, they potentially represent hybrid neurons capable of GABA/glutamate corelease, as characterized in the hypothalamus and a few other brain

*Howard Hughes Medical Institute, Harvard University, Cambridge, MA 02138, USA. [†]Department of Chemistry and Chemical Biology, Harvard University, Cambridge, MA 02138, USA.

[‡]Department of Physics, Harvard University, Cambridge, MA 02138, USA. [§]Center for Brain Science, Harvard University, Cambridge, MA 02138, USA. [¶]Department of Molecular and Cellular Biology, Harvard University, Cambridge, MA 02138, USA. ^{||}Klarman Cell Observatory, Broad Institute of MIT and Harvard, Cambridge, MA 02139, USA. [¶]Koch Institute of Integrative Cancer Biology, Department of Biology, MIT, Cambridge, MA 02139, USA.

^{*}These authors contributed equally to this work. [†]These authors contributed equally to this work. [‡]These authors contributed equally to this work. ^{||}These authors contributed equally to this work. [¶]Corresponding author. Email: dulac@fas.harvard.edu (C.D.); zhuang@chemistry.harvard.edu (X.Z.).

^{*}These authors contributed equally to this work. [†]These authors contributed equally to this work. [‡]These authors contributed equally to this work. ^{||}These authors contributed equally to this work. [¶]Corresponding author. Email: dulac@fas.harvard.edu (C.D.); zhuang@chemistry.harvard.edu (X.Z.).

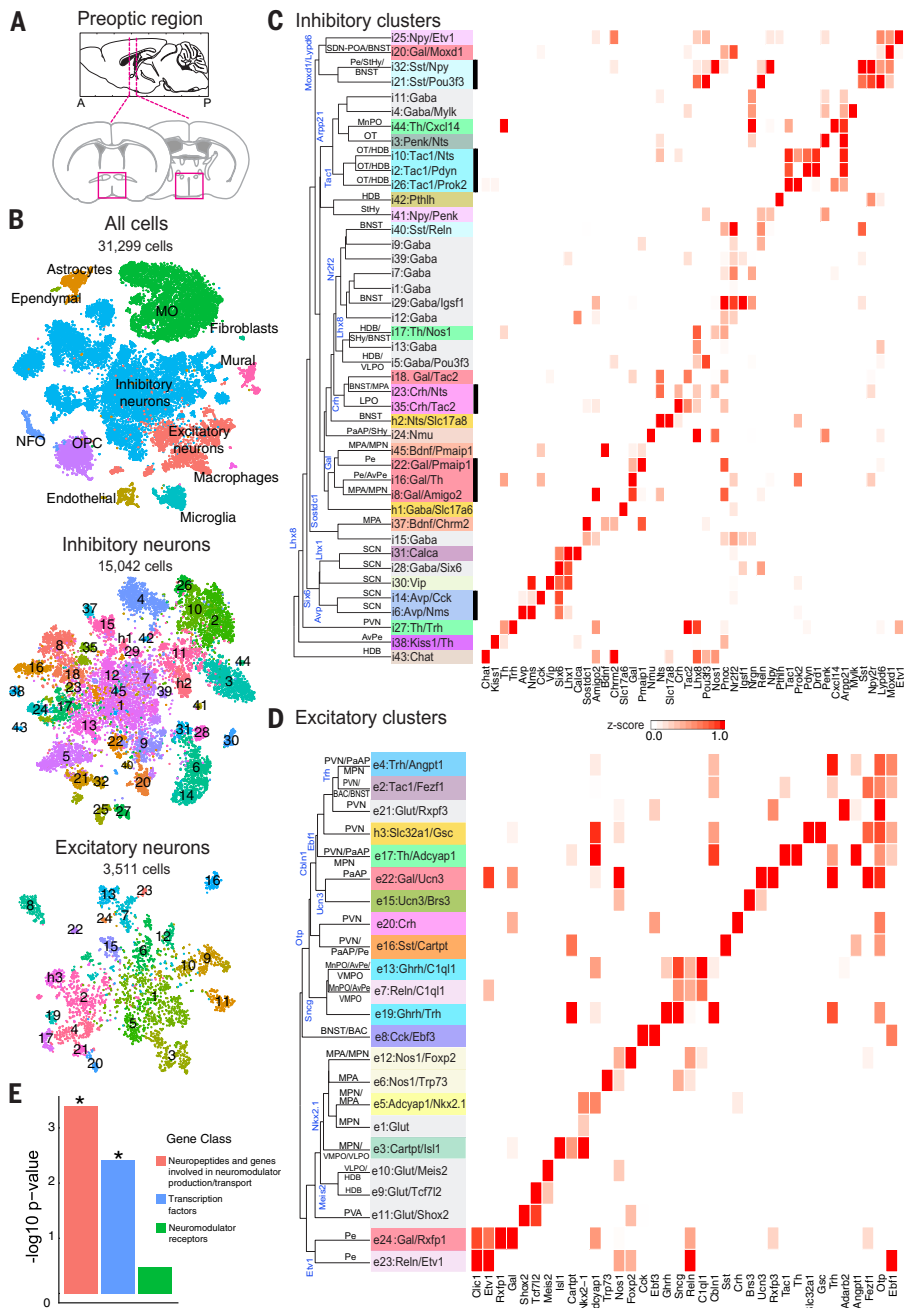


Fig. 1. scRNA-seq of the preoptic region in the mouse hypothalamus. (A) Schematic of the preoptic region of the hypothalamus. Magenta boxes indicate the area dissected for scRNA-seq (Bregma +0.5 to -0.6). (B) t-distributed stochastic neighbor embedding (tSNE) for all cells and inhibitory and excitatory neurons, with cells colored by cluster. Numbers superimposed on the tSNE indicate the cluster ID. Total cell numbers for each tSNE plot are indicated. NFO, newly formed oligodendrocytes; OPC, oligodendrocyte progenitor cells; MO, mature oligodendrocytes. (C) Heat map of z-scores of expression for select genes within inhibitory neuronal clusters. Clusters are organized on the basis of the hierarchical tree constructed with expression in principal component space, with some of the genes differentially expressed between branches indicated (blue). The nomenclature of clusters uses a numeric indicator of excitatory or inhibitory cluster followed by one or two marker genes, with the first marker typically a neuromodulator (29). Inhibitory and excitatory clusters that lack a notable neuromodulator marker gene were designated as Gaba and Glut, respectively, with an additional marker gene to help differentiate among these clusters when possible. Cluster names are colored according to the first gene. Predicted anatomical locations for the clusters are listed on the tree, and the unlabeled lines indicate that such prediction was not possible. Thick black lines underscore clusters grouped by common neuropeptide expression. (D) As in (C) but for excitatory neurons. The hybrid neuronal clusters h1/h2 and h3 are listed in (C) and (D), respectively, because they were initially classified as inhibitory and excitatory, respectively. (E) $-\log_{10}(P \text{ value})$ for the enrichment of gene categories in differentially expressed genes that mark neuronal clusters calculated based on a gene-set enrichment analysis as shown in fig. S6. * $P < 0.05$.

regions (32–34). We denote these clusters as h1, h2, and h3 (Figs. 1, C and D, and fig. S3C).

To determine the gene categories that best discriminate neuronal clusters, we examined the top five most differentially expressed genes in each cluster and observed enrichment for neuropeptides and molecules involved in neuromodulator production and transport, as well as for transcription factors, but not for neuromodulator (neuropeptide and hormone) receptors. Quantitative analyses of enrichment profiles of these three gene classes among differentially expressed genes further support this notion (Fig. 1E, fig. S6, and table S3). Neuromodulator receptors did discriminate some clusters (for example, Npr1, Rxfp1, Brs3, and Drd1) (Fig. 1, C and D, and figs.

S4 and S5). However, on average, neuromodulator receptors were expressed more widely and at lower levels than neuromodulators and transcription factors, limiting their use as potential markers for functional studies. Most clusters were discriminated by combinations of genes rather than by single markers.

Hierarchical tree analyses (29) showed that inhibitory neuronal clusters that express a common neuromodulator were often grouped together on the tree—for example, clusters expressing Avp, Gal, Crh, Tacl, and Sst (Fig. 1C)—suggesting potential functional or developmental commonality among them. By contrast, neuromodulators largely failed to group excitatory neuronal clusters (Fig. 1D). Instead, predicted locations of in-

dividual clusters on the basis of spatial expression patterns of their marker genes observed in the Allen Brain Atlas (35) and our own *in situ* hybridization data (fig. S7) suggest that excitatory clusters tended to be grouped on the tree by anatomical structures or nuclei (Fig. 1D). For example, markers of clusters e4, e2, e21, h3, and e17 defined a node in the tree located in the PVN and adjacent nuclei (MPN, PaAP, BAC, and BNST), markers of node-sharing clusters e13 and e7 placed these populations in the MnPO/AvPe/VMPPO region, whereas markers of e12, e6, e5, and e1 placed these cells in the MPN/MPA region (Fig. 1D) (full names of the nuclei described in this work are provided in table S4). We thus hypothesize that excitatory neuron types tend to be spatially segregated

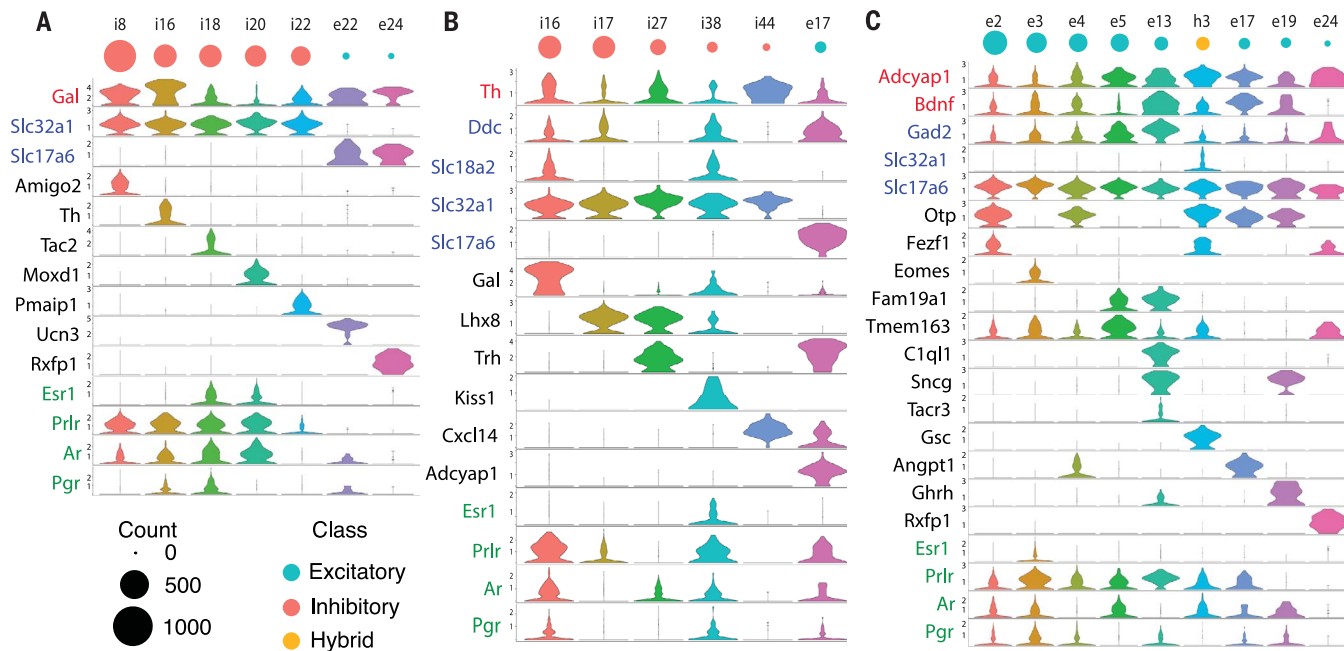


Fig. 2. scRNA-seq identifies subdivisions of cells that express markers previously associated with single neuronal populations. (A to C) Expression distributions of selected marker genes and genes of interest in all neuronal clusters that are statistically enriched [Model-based Analysis of Single-cell Transcriptomics (MAST) (25), false discovery rate <0.01] in (A) galanin (Gal), (B) tyrosine hydroxylase (Th), or (C) Bdnf and Adcyap1. Gene names in black indicate differentially expressed genes for each se-

lected neuronal cluster. Gene names in blue indicate inhibitory (Gad1, Gad2, Slc32a1) and excitatory (Slc17a6) neuronal markers, as well as dopaminergic markers (Ddc, Slc6a3, and Slc18a2). Gene names in green indicate sex hormone receptors. The y axis on each violin plot depicts the log transformed counts with the range set to the 95% expression quantile of the cluster with the highest expression (29). The sizes of red, cyan, and yellow circles correspond to the cell abundance of the inhibitory, excitatory, and hybrid clusters, respectively.

in distinct anatomical structures of the preoptic region, in a manner similar to the spatial segregation of different types of excitatory neurons in various layers of the cortex (36). Similar analysis with the inhibitory neuronal tree suggests that although some groups of clusters were defined by spatially restricted transcription factor expression—for example, Six6 marking the SCN (Fig. 1C)—such spatial grouping of transcriptionally similar clusters appeared to be less pronounced than with excitatory clusters. Additionally, transcription factors tended to mark groups of neuronal clusters further subdivided by neuromodulator expression (Fig. 1, C and D), which is consistent with earlier reports of hypothalamic parcellation by transcription factors during early development (37).

Specific neuronal clusters identified with scRNA-seq

Previous studies of the preoptic region have defined cell populations associated with the regulation of specific homeostatic and behavioral functions on the basis of the expression of one or more marker genes (table S5). Clusters that express these marker combinations were identified in our scRNA-seq data (figs. S4 and S5), together with many previously unknown cell populations. Moreover, we uncovered a high level of molecular heterogeneity among a number of previously reported singular cell types, thus partitioning them into multiple distinct populations, as illustrated below on specific examples.

The neuropeptide galanin (Gal) has been associated with behaviorally relevant cell populations of the preoptic region (4, 5, 38) in the MPOA (parenting and feeding) (5, 38) and VLPO (sleep) (4). Our scRNA-seq data revealed seven neuronal clusters that were statistically enriched in Gal expression, each characterized by distinct marker genes (Fig. 2A) validated with two-color *in situ* hybridization (fig. S7A). These clusters were each associated with different hormonal modulations, ranging from cluster i20:Gal/Moxd1, predicted to lie in the sexually dimorphic nucleus of the POA (Fig. 1C) and expressing a wide range of sex steroid and neuropeptide receptors, to cluster e24:Gal/Rxfp1, expressing no sex steroid receptor (Fig. 2A).

Second, cells that express tyrosine hydroxylase (Th), a key enzyme involved in catecholamine synthesis, have been viewed as a single population involved in several social behaviors (6, 39). We identified six Th-enriched neuronal clusters (Fig. 2B and fig. S7B), among which only i16:Gal/Th and i38:Kiss1/Th expressed both Dopa decarboxylase (Ddc) and the vesicular monoamine transporter Vmat2 (Slc18a2), genes required for dopaminergic function (Fig. 2B).

Last, the neuropeptide adenylate cyclase activating polypeptide 1 (Adcyap1) and brain-derived neurotrophic factor (Bdnf) have recently been identified as combined markers for preoptic neurons sensing warm temperature (8). Our data revealed nine Adcyap1- and Bdnf-enriched clusters (Fig. 2C). Although the warm-sensitive neurons

have been previously considered as inhibitory neurons on the basis of their functional properties and expression of Gad2, all nine Adcyap1- and Bdnf-enriched clusters identified here coexpressed Gad2 and Slc17a6, and only one of them also expressed Slc32a1 (Fig. 2C), identifying these clusters as excitatory or hybrid neurons. We further identified one of these clusters as representing warm-sensitive neurons with the help of MERFISH. A recent study has revealed that a neuronal population that controls thirst-motivated behavior also expresses Adcyap1 and Bdnf (10), further supporting the notion that Adcyap1 and Bdnf are imperfect markers for warm-sensitive cells.

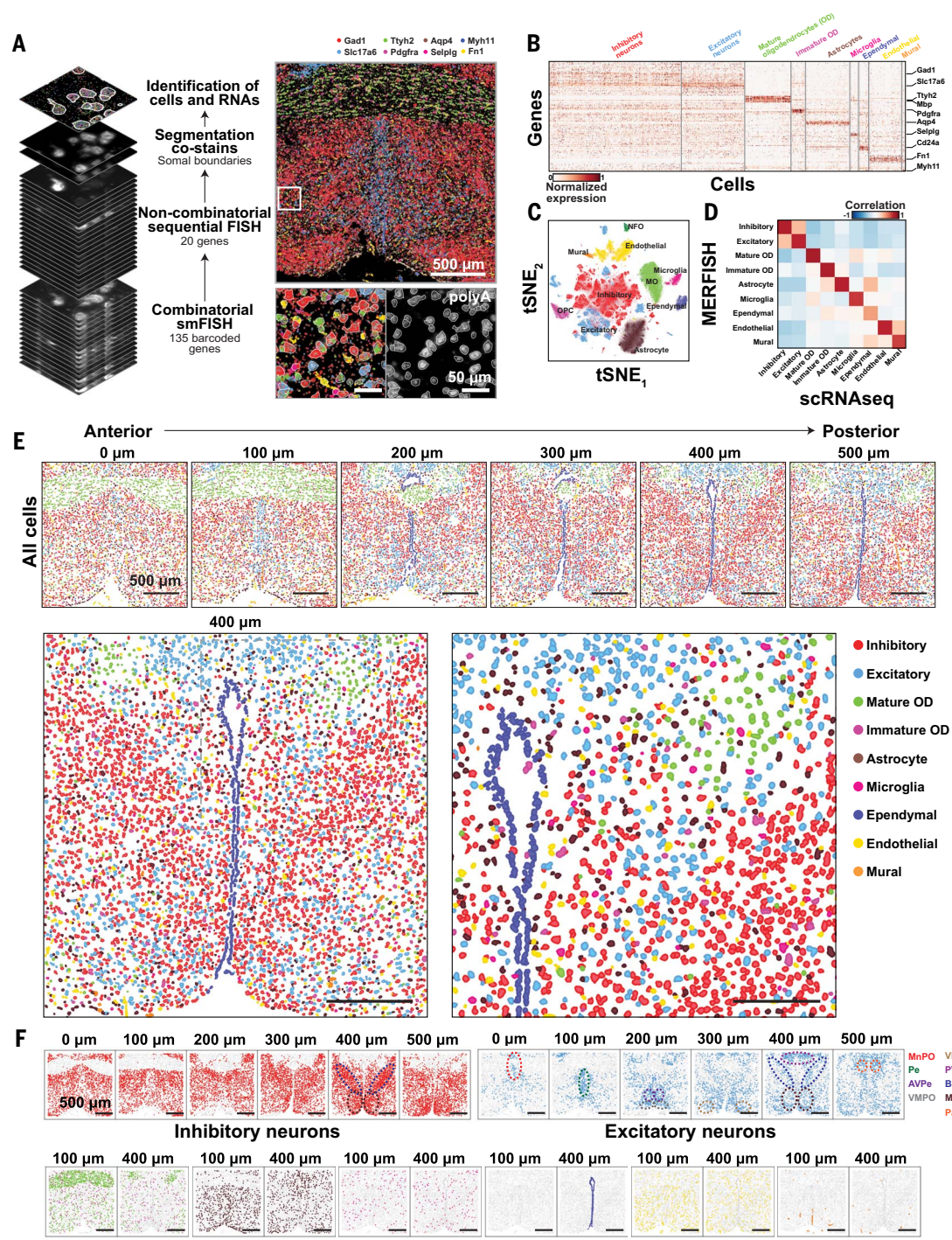
MERFISH measurements of the preoptic region

Next, we performed MERFISH measurements of the preoptic region (1.8 by 1.8 by 0.6 mm, Bregma +0.26 to -0.34), within the area characterized with scRNA-seq, targeting a set of 155 genes (Fig. 3A and table S6) (29). These genes were composed of two groups: (i) 85 preselected genes that were either known markers for major cell classes or relevant to neuronal functions of the hypothalamus, such as neuropeptides and neuromodulator receptors, and (ii) 70 additional genes that were identified with scRNA-seq as neuronal cluster markers but not already included in the 85 preselected genes. Among these 155 genes, 135 genes were imaged by using combinatorial smFISH with an error-robust barcoding scheme, as demonstrated previously for MERFISH (20, 26, 40). The

Fig. 3. Major cell classes and their spatial organizations in the preoptic region as revealed with MERFISH. (A) (Left)

Schematic of the MERFISH measurements. Combinatorial smFISH imaging was used to identify 135 genes, followed by sequential rounds of two-color FISH to identify 20 additional genes. Total polyadenylated mRNA and nuclei costains then allowed cell boundary segmentation. (Top right) Pseudo-colored dots marking localizations of individual molecules of eight example RNA species, each marking a distinct major cell class, in a 10- μm -thick, 1.8- by 1.8-mm slice. (Bottom right) Magnification of the white boxed region (left) and the total mRNA image and the segmented cell boundaries of the same region (right). The raw and decoded MERFISH images of the same field of view (FOV) for all 135 genes measured by using combinatorial smFISH are shown in fig. S9; the total mRNA and nuclei costain images and segmented cell boundaries for the same FOV are shown in fig. S10. The segmented cell boundaries represent the boundaries of the cell soma (29). A subset of identified RNA molecules fell outside these boundaries and are thus candidates for RNAs in neuronal or glial processes. (B) Expression of all genes measured with MERFISH for ~500,000 cells imaged in multiple naïve animals.

Expression for each gene is normalized to the 95% expression quantile for that gene across all cells. Cells are grouped by major classes, and markers of each major cell class are listed on the right. OD, oligodendrocytes. (C) tSNE plot of these cells. (D) Pairwise Pearson correlation coefficients between the average expression profiles (in z-scores) of individual cell classes identified with MERFISH and scRNA-seq. (E) (Top) Spatial distribution of all major cell classes across sections at different anterior-posterior positions from a single female mouse. Cells are marked with cell segmentation boundaries and colored by cell classes as indicated. Six of the twelve 1.8- by 1.8-mm imaged slices are shown. The 0, 100, 200, 300, 400, and 500 μm labels indicate the distance from the anterior position (Bregma +0.26). (Bottom) Enlarged image of the slice at 400 μm from the anterior position (left) and a further magnified image of the region shown in the gray dashed box (right). Scale bars, 500 μm (left), 250 μm (right). (F) Spatial distributions of individual cell classes are shown as colored dots on the background of all cells shown as gray dots. Dashed ovals indicate several specific hypothalamic nuclei and are colored identically to the nuclei abbreviations listed to the right. BNST, bed nucleus of the stria terminalis; MPN, medial preoptic nucleus; MnPO, median preoptic nucleus; Pe, periventricular hypothalamic nucleus; AvPe, anteroventral periventricular nucleus; VMPO, ventromedial preoptic nucleus; VLPO, ventrolateral preoptic nucleus; PVA, paraventricular thalamic nucleus; PaAP, paraventricular hypothalamic nucleus, anterior parvicellular.



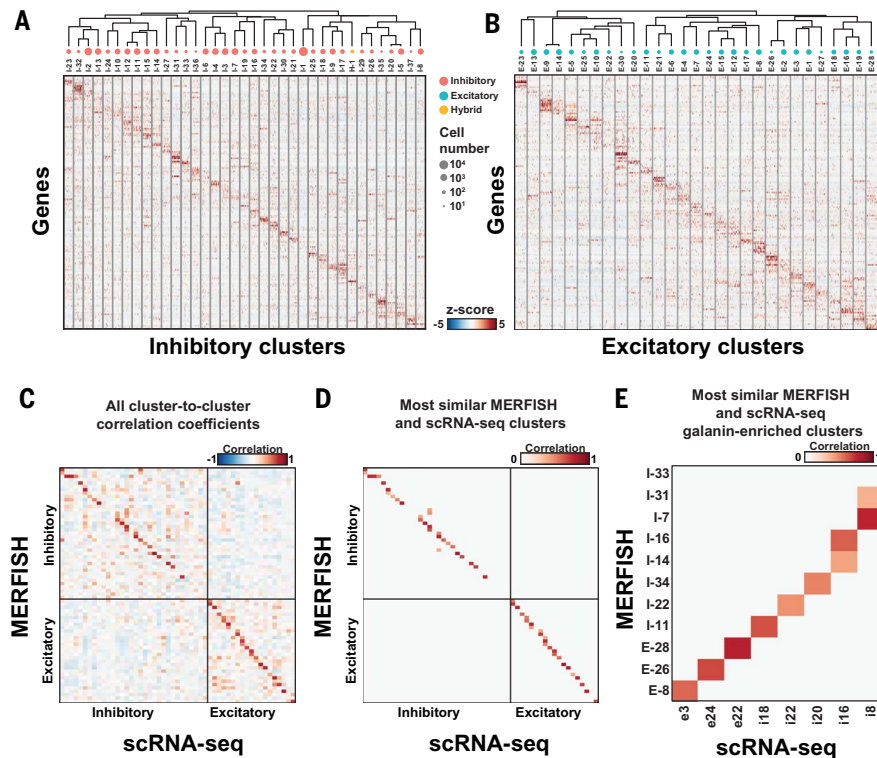


Fig. 4. Neuronal clusters in the preoptic region as revealed with MERFISH. (A and B) z-scores of expression profiles for (A) inhibitory and (B) excitatory neuronal clusters identified with MERFISH. Depicted are 100 random cells from each cluster. The neuronal clusters are organized on the basis of similarity in their expression profiles, as depicted by the dendrogram. The sizes of red, cyan, and yellow circles indicate the abundance of neuronal clusters, and only clusters with more than 100 cells are depicted. H-1 is grouped with the inhibitory clusters because it was initially classified as inhibitory neurons. (C) The pairwise Pearson correlation coefficients between the expression profile (in z-score) of the MERFISH and scRNA-seq clusters. The order of the clusters in (C) is not the same as in (A) and (B). (D) As in (C) but with only scRNA-seq cluster(s) most similar to each MERFISH cluster shown, identified as the cluster(s) with the highest Pearson correlation coefficient(s) (fig. S14 and table S9) (29). When multiple scRNA-seq clusters show statistically indistinguishable, highest correlation coefficients to a MERFISH cluster (29), all of them are indicated. scRNA-seq clusters outside the region imaged with MERFISH, as assessed by the expression patterns of the marker genes in the Allen Brain Atlas (35) and our own in situ data (fig. S7) (29), are excluded from this analysis (29). (E) Same as (D) but for clusters enriched in galanin (Gal).

remaining 20 genes were relatively short and/or expressed at high levels, which is challenging for combinatorial smFISH detection, and hence were measured in sequential rounds of multicolor FISH after the combinatorial run. The sexually dimorphic expression previously reported for 11 genes (41, 42) was confirmed here (fig. S8).

We sectioned the preoptic region into 60 evenly spaced slices along the anterior-posterior axis and performed three-dimensional MERFISH imaging on every fifth slice (29). Individual RNA molecules were clearly detected and identified (fig. S9), and individual cells were segmented based on 4',6-diamidino-2-phenylindole (DAPI) and total mRNA staining (fig. S10) (29). In total, we profiled >400,000 cells from three to four replicates in naïve male and female animals, as well as >500,000 additional cells from three to five replicates of animals subjected to behavioral stimuli (29). MERFISH expression data showed high reproducibility between replicates

(fig. S11A), good correlation with bulk RNA-seq data of the preoptic region (43) (fig. S11B), and a low false-detection rate (fig. S11C). For the targeted genes, MERFISH detected on average six to eightfold more transcript copies per cell than did scRNA-seq (fig. S12, A to D), underscoring the high sensitivity of MERFISH.

We used an unsupervised, community-detection-based clustering approach similar to that applied to scRNA-seq data to identify transcriptionally distinct cell populations in MERFISH data (Fig. 3, B and C, and table S7) (29). MERFISH identified all major cell classes (Fig. 3, B and C), except for macrophages and fibroblasts, potentially because the corresponding marker genes were not included in the MERFISH gene library. The expression profiles of cell classes measured with MERFISH were strongly correlated with those determined by using scRNA-seq (Fig. 3D). However, the relative abundance of cells in various cell classes differed in the two datasets (fig. S12E). In partic-

ular, astrocytes, endothelial cells, and ependymal cells were depleted in our scRNA-seq data, presumably because of cell loss during tissue dissociation.

MERFISH also provided a direct measurement of the spatial distribution of major cell classes. As expected, mature oligodendrocytes were enriched in the anterior commissure and the fornix-major myelinated fiber tracts of the rostral hypothalamus, whereas immature oligodendrocytes, astrocytes, microglia, and endothelial cells were dispersed throughout (Fig. 3, E and F). Ependymal cells formed a single layer lining the more caudal aspects of the third ventricle, and mural cells were organized in veriform structures that resemble blood vessels (Fig. 3, E and F). Notably, inhibitory and excitatory neurons exhibited distinct distributions (Fig. 3, E and F). Inhibitory neurons, the more abundant neuronal type in the preoptic region, were widely dispersed across this region but enriched in specific posterior nuclei, including the BNST and MPN. By contrast, excitatory neurons were specifically enriched in a few nuclei anteriorly but became more dispersed posteriorly and, in agreement with previous reports (44), were depleted in the posterior BNST.

MERFISH analyses of specific neuronal types

Clustering analyses of inhibitory neurons and excitatory neurons separately identified ~40 inhibitory and ~30 excitatory neuronal populations (Fig. 4, A and B, and tables S7 and S8). We investigated the impact of the number of genes used to cluster cells in MERFISH data and found that ~90% of the identified neuronal clusters were recovered by using the ~75 genes that were most informative among the 155 (fig. S13). Beyond this point, cluster recovery increased more slowly with the number of genes added (fig. S13). Hereafter, we denote excitatory and inhibitory neuronal clusters identified with MERFISH as E-1, E-2, ... and I-1, I-2, ..., respectively, and the one identified hybrid cluster as H-1.

The expression profiles of most neuronal clusters determined with MERFISH correlated well with those of scRNA-seq clusters (Fig. 4C and fig. S14, A and B). This observation allowed us to infer, for each MERFISH cluster, the putative corresponding or most similar scRNA-seq cluster(s), defined as the cluster(s) with the highest correlation coefficient(s) (Fig. 4D, fig. S14C, and table S9) (29), which could help expand our knowledge of the expression profiles of the MERFISH clusters. Similar correspondence was observed by using a neural network classifier (fig. S14, D and E). Correlations between MERFISH and scRNA-seq clusters were only moderately weaker than those between scRNA-seq clusters derived from bootstrapped replicates (fig. S14, F and G). Many MERFISH clusters had a distinct, most similar scRNA-seq cluster (Fig. 4D, fig. S14, and table S9). However, in some instances, multiple MERFISH clusters exhibited the highest correlation to the same scRNA-seq cluster; in addition, a small fraction of MERFISH clusters lacked a statistically significant correlation to any scRNA-seq cluster (Figs. 4D, fig. S14, and table S9). Both of these

scenarios suggest that some clusters identified with MERFISH were not discriminated by scRNA-seq. Conversely, a small fraction of scRNA-seq clusters lacked a statistically significant correlation to any MERFISH cluster (Fig. 4D, fig. S14, and table S9), suggesting that these clusters were not identifiable by the MERFISH gene panel or were located outside the MERFISH-imaged area (29).

As a specific illustration, MERFISH identified 10 clusters enriched in Gal expression, some showing one-to-one correspondences to Gal-enriched scRNA-seq clusters (Fig. 4E; fig. S15, A and B; and table S9). We also observed instances in which two Gal-enriched MERFISH clusters putatively corresponded to the same Gal-enriched scRNA-seq cluster (for example, I-14 and I-16 to i16) (Fig. 4E and table S9), suggesting that MERFISH resolved subpopulations within the scRNA-seq cluster. Indeed, we identified two subsets of cells within the scRNA-seq cluster i16, each respectively expressing markers of the MERFISH clusters I-14 and I-16 (fig. S15, C and D). The calcitonin receptor (Calcr)- and bombesin receptor (Brs3)-positive I-14 and the Th-positive I-16 were found to be differentially activated in specific social behaviors, as described later (table S9), supporting the resolution of these cells into two distinct populations. We also observed a similar resolution of i8 into I-7 and I-31 (Fig. 4E; fig. S15, E and F; and table S9). A Gal-enriched scRNA-seq cluster could also be split into Gal-enriched and non-Gal-enriched MERFISH clusters [for example, i20 into Gal-enriched cluster I-34 and non-Gal-enriched clusters I-2 and I-32 (fig. S15, G and H, and table S9)].

Examination of the MERFISH or scRNA-seq clusters that were not discriminated by the other method showed several trends. Some of the MERFISH clusters not detected with scRNA-seq had relatively low abundance and thus might not be sufficiently represented in our scRNA-seq data, which profiled 4% as many neurons as we did in MERFISH. Some of the MERFISH clusters not discriminated by scRNA-seq had lowly expressed marker genes, which may not be reliably detected with scRNA-seq. Conversely, some scRNA-seq clusters not identified with MERFISH had marker genes that were not included in the MERFISH gene library. Some of the extremely low-abundance MERFISH or scRNA-seq clusters that lack correspondence may not represent well-identified clusters. These results thus demonstrate the complementary nature of MERFISH and scRNA-seq and an increased ability to characterize cell populations when both approaches are combined. Nevertheless, some clusters still exhibited heterogeneity in gene expression associated with distinct spatial locations (fig. S16), suggesting either spatial gradients in gene expression within the same cluster or the presence of unresolved cell subpopulations.

Spatial organization of specific neuronal cell types

Next, we examined the spatial distributions of individual neuronal clusters (Fig. 5A and figs. S17 and S18) within the framework of major anatomically defined nuclei of the preoptic region

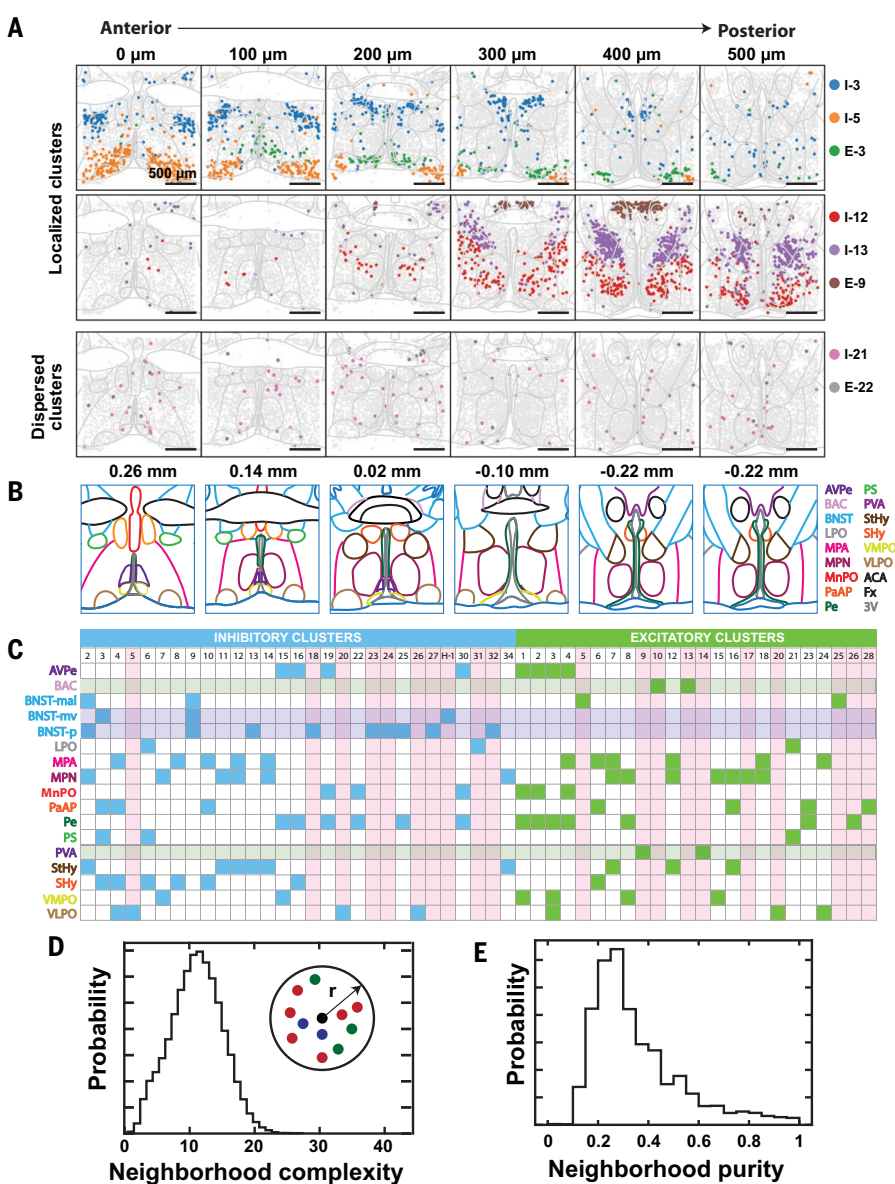


Fig. 5. The spatial organization of neuronal clusters in the preoptic region. (A) Spatial distribution of example neuronal clusters that are localized (top and middle) or dispersed (bottom). Depicted are six of the 12 slices imaged from a female mouse. Colored markers indicate cells of the specified neuronal clusters, and gray markers indicate all other neurons. Nuclei boundaries depicted in light gray are drawn according to (45) and aligned to the tissue slices according to the locations of landmarks, such as the anterior commissure, fornix, and ventricle. The 0, 100, 200, 300, 400, and 500 μm labels indicate the distance from the anterior position (Bregma +0.26). (B) Illustration of major hypothalamic nuclei spanning the imaged region and colored according to legend on the right (45). Nuclei abbreviations are as defined in Fig. 3F, and additionally, BAC, bed nucleus of the anterior commissure; LPO, lateral preoptic area; MPA, medial preoptic area; PS, parastrial nucleus; StHy, striohypothalamic nucleus; SHy, septohypothalamic nucleus; ACA, anterior commissure; Fx, fornix; 3V, third ventricle. Bregma locations are listed on top and the map at Bregma -0.22 is duplicated. (C) Summary of nuclei in which inhibitory (blue) or excitatory (green) neuronal clusters are enriched. Translucent horizontal bars indicate nuclei that contain only inhibitory (blue) or excitatory (green) clusters. Vertical pink bars highlight clusters primarily enriched in single nuclei. BNST-mal, BNST, medial division, anterolateral part; BNST-mv, BNST, medial division, ventral part; BNST-p, BNST, posterior part. (D) and (E) Analysis of spatial mixing of distinct neuronal clusters. We define the complexity of the neighborhood surrounding any given neuron as the number of distinct neuronal clusters present within that neighborhood, and the purity of that neighborhood as the fraction of all cells within the given neighborhood that are part of the most abundant cluster. Probability distributions of the complexity (D) and purity (E) of the 100-μm-radius neighborhood surrounding any given neuron are depicted.

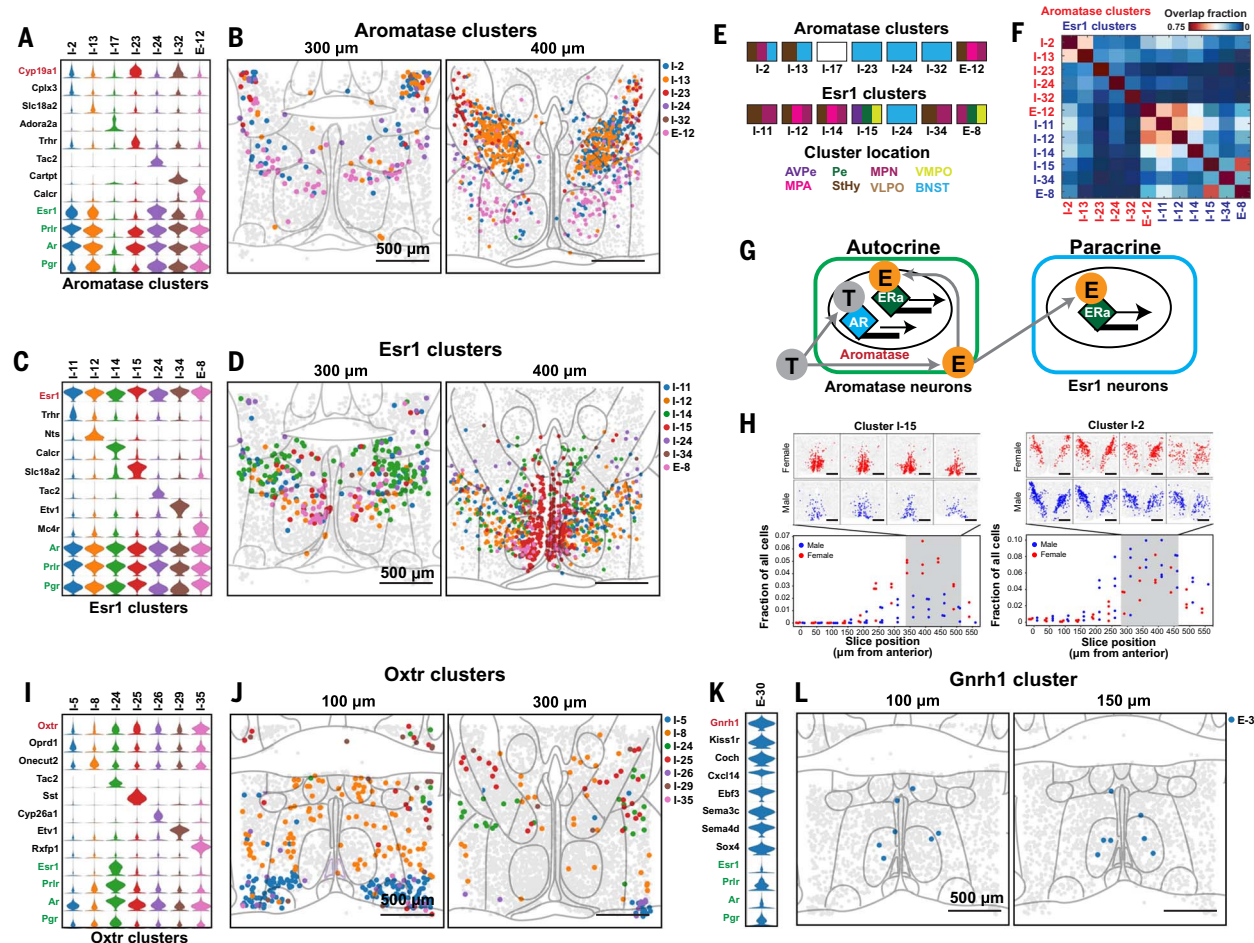


Fig. 6. Spatial and molecular organization of neuronal clusters enriched in genes relevant to social behaviors. (A) Expression distributions of selected marker genes and genes of interest for neuronal clusters enriched in aromatase (*Cyp19a1*). Expression distributions are calculated as in Fig. 2. (B) Spatial distributions of neuronal clusters depicted in (A). Two of the 12 slices from a female mouse sample are depicted. Nuclei boundaries depicted in light gray are as defined in Fig. 5A. (C and D) As in (A) and (B) but for clusters enriched in estrogen receptor α (*Esr1*). (E) Schematic showing the nuclei spanned by individual clusters, as indicated by the color subdivisions of the rectangles, colored identically to the nuclei abbreviations listed below. The nuclei abbreviations are as defined in Figs. 3F and 5B. I-17 is not colored because it was found at the edge of our imaged region and falls outside of the boundaries of the nearest imaged nuclei, the VLPO (table S9). (F) Average overlap fraction between aromatase-enriched clusters and *Esr1*-enriched clusters for all measured animals. Cluster I-24 is enriched in both aromatase

and *Esr1* and listed only once. (G) Models of autocrine and paracrine signaling. Circulating testosterone (gray T) can activate cells expressing androgen receptor (AR) or, in cells expressing aromatase, can be converted to estrogen (orange E). Autocrine: In cells co-expressing aromatase and *Esr1*, estrogen produced in these cells can activate estrogen receptor (ER α) in the same cells. Paracrine: Estrogen produced by aromatase-enriched cells can activate ER α in nearby cells enriched with *Esr1*. (H) Comparison of the fraction of cells that belong to the specified neuronal clusters (I-15 or I-2) for all male (blue) and female (red) replicates as a function of the anterior-posterior position of the slices. Above each panel are the spatial distribution of the cluster in four slices from a single female (red) and male (blue) replicate. (I and J) As in (A) and (B) but for clusters enriched in oxytocin receptor (*Oxtr*). (K and L) As in (A) and (B) but for a cluster enriched in gonadotropin-releasing hormone 1 (*GnRH1*). MERFISH revealed 8, 15, and 19 aromatase-, *Esr1*- and *Oxtr*-enriched clusters, respectively, with only the seven most enriched clusters depicted for each.

as depicted in Fig. 5B (45). About 30% of the MERFISH clusters were enriched primarily in a single nucleus (Fig. 5C, pink shading)—for example, cluster I-5 primarily in the VLPO and cluster E-9 in the PVA (Fig. 5, A to C)—whereas approximately half of the clusters were distributed over a few (two to four), often physically contiguous nuclei (Fig. 5C, unshaded clusters)—for example, cluster I-3 in the BNST-mv, PaAP, PS, and SHy and cluster I-12 in the StHy, MPA, and MPN (Fig. 5, A to C). This anatomical dispersion may reflect a similar function of the same cell type across distinct nuclei or a developmental relationship of spatially distinct cells. By contrast,

small fraction of the neuronal clusters were dispersed and not enriched in any given nucleus, such as I-21 and E-22 (Fig. 5A). Whereas most nuclei were populated by both excitatory and inhibitory neurons, the PVA and BAC only contained excitatory clusters (Fig. 5C, green shaded row), and the BNST-p and BNST-mv contained only inhibitory clusters (Fig. 5C, blue shaded rows), which is consistent with previous observations of high expression of *Slc17a6* and *Slc32a1* in these regions, respectively (35, 44).

Neuronal clusters of the preoptic region appeared highly intermixed, with multiple clusters occupying any given nucleus. To quantify the

degree of intermixing, we calculated the neighborhood composition for each neuron. This analysis showed that each neighborhood contained multiple clusters and was typically not dominated by a single cell population (Fig. 5, D and E).

These direct spatial measurements allowed us to provide an anatomy-based taxonomy for the identified neuronal clusters, except for the dispersed clusters, which we named on the basis of marker genes (table S9). The putative correspondence between these MERFISH clusters and scRNA-seq clusters allowed us to further assess the spatial locations of scRNA-seq clusters and compare them with our earlier predictions

shown in Fig. 1, C and D. In nearly all cases, the predicted locations matched or partially overlapped those of the corresponding MERFISH clusters (table S9), lending additional support to our earlier observations on the spatial relationship between transcriptionally similar clusters (Fig. 1, C and D). However, we caution that the predicted scRNA-seq cluster locations represent rough approximations because of the relatively low resolution of available *in situ* hybridization data and suffer from occasional ambiguity in the spatial patterns of some marker genes. Moreover, because of the remaining heterogeneity in some of the identified scRNA-seq and MERFISH clusters, the putative correspondence may only represent similarity between subsets of cells within these clusters.

Spatial and molecular organization of socially relevant cell populations

Neuromodulators, hormones, and associated signaling pathways play critical roles in hypothalamic functions, but analyses with cellular resolution have been limited owing to the low expression level of many of the corresponding receptors. MERFISH enabled us to examine the distribution of these genes throughout the preoptic region, providing functional insights into the associated cell populations.

Sex steroid hormones are essential to the development and modulation of social behaviors and reproduction. We examined the distribution of enzymes and receptors essential for steroid hormone signaling in the preoptic region. The enzyme aromatase (*Cyp19a1*) converts testosterone to estrogen and thus modulates steroid function (39). MERFISH revealed aromatase-enriched clusters with distinct repertoires of sex hormone receptors (Fig. 6, A and B). Several of these clusters (such as I-2, I-13, I-24, I-32, and E-12) expressed both androgen receptor (Ar) and estrogen receptor α (*Esr1*), suggesting that in these cell populations, circulating testosterone can be converted into estrogen and thus affect gene expression in a cell-autonomous manner through *Esr1* activation. In addition, the aromatase-enriched clusters E-12 and I-2 substantially overlapped with locations of several *Esr1*-enriched clusters (Fig. 6, C to F), suggesting that estrogen synthesized by these aromatase-expressing cells may also act in a paracrine manner on cells of the nearby *Esr1*-enriched clusters, in addition to the autocrine signaling mode described above (Fig. 6G).

Some *Esr1*-enriched and aromatase-enriched clusters exhibited differences in cell abundance of varying extent between males and females. For example, the *Esr1*-enriched cluster I-15 showed an appreciable enrichment in female animals, whereas the aromatase-enriched cluster I-2 showed a more modest male enrichment (Fig. 6H). I-2 overlapped with the sexually dimorphic nucleus of the preoptic area (SDN-POA), and its marker gene *Cpx3* was co-expressed with *MoxD1* [a canonical SDN-POA marker (46) not in our MERFISH gene library] in cells of the SDN-POA and BNST (fig. S19). However, I-2:BNST/StHy/MPN spatially extended beyond the boundaries of the SDN-POA,

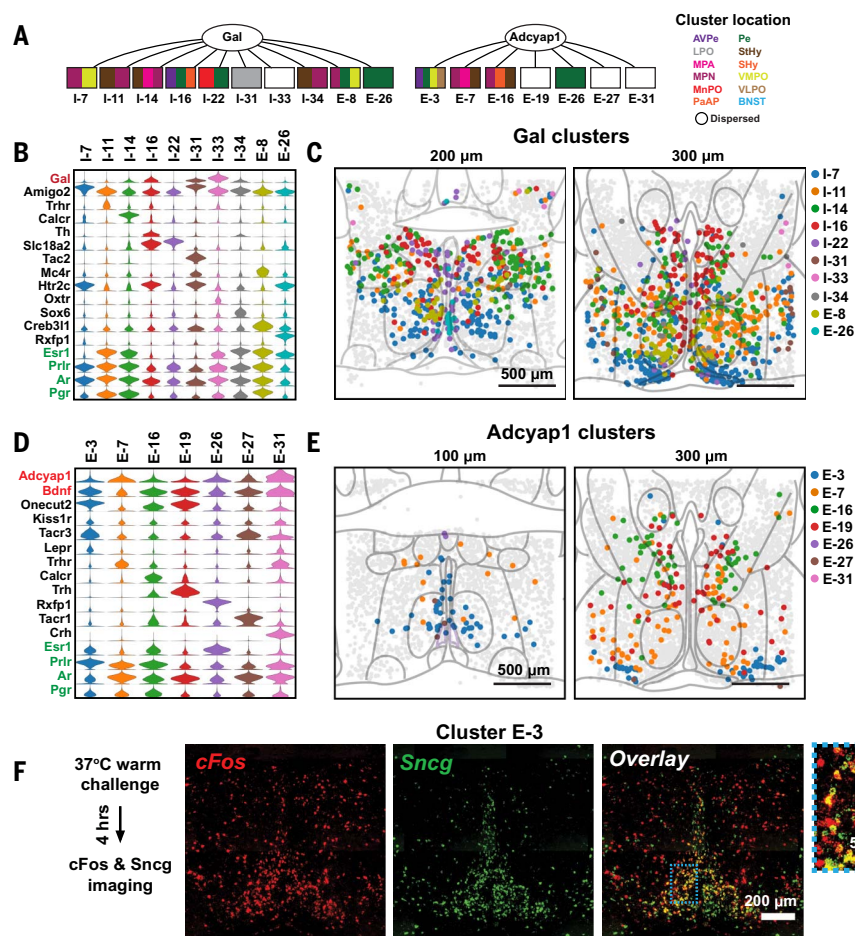


Fig. 7. Subdivisions of neuronal populations expressing Gal or Adcyap1 revealed with MERFISH. (A) MERFISH subdivides galanin- and Adcyap1-expressing cells into multiple transcriptionally and spatially distinct clusters. Color subdivision of the rectangles shows the nuclei spanned by individual clusters, colored identically to the nuclei abbreviations listed on the right. The nuclei abbreviations are as defined in Figs. 3F and 5B. (B) Expression distributions of selected marker genes and genes of interest for all neuronal clusters enriched in galanin (Gal). Expression distributions are calculated as in Fig. 2. (C) Spatial distributions of all inhibitory and excitatory Gal-enriched clusters. (D) As in (B) and (C) but for Adcyap1- and Bdnf-enriched clusters. The seven most enriched of the 14 Adcyap1- and Bdnf-enriched clusters are shown. (E) *In situ* hybridization images of cFos (red), Sncg (green), and overlay of an anterior slice of the preoptic region taken from a heat-stressed animal. The blue boxed region is magnified and shown on the right. Sncg is a marker for the scRNA-seq cluster e13 that corresponds to the MERFISH cluster E-3 (table S9).

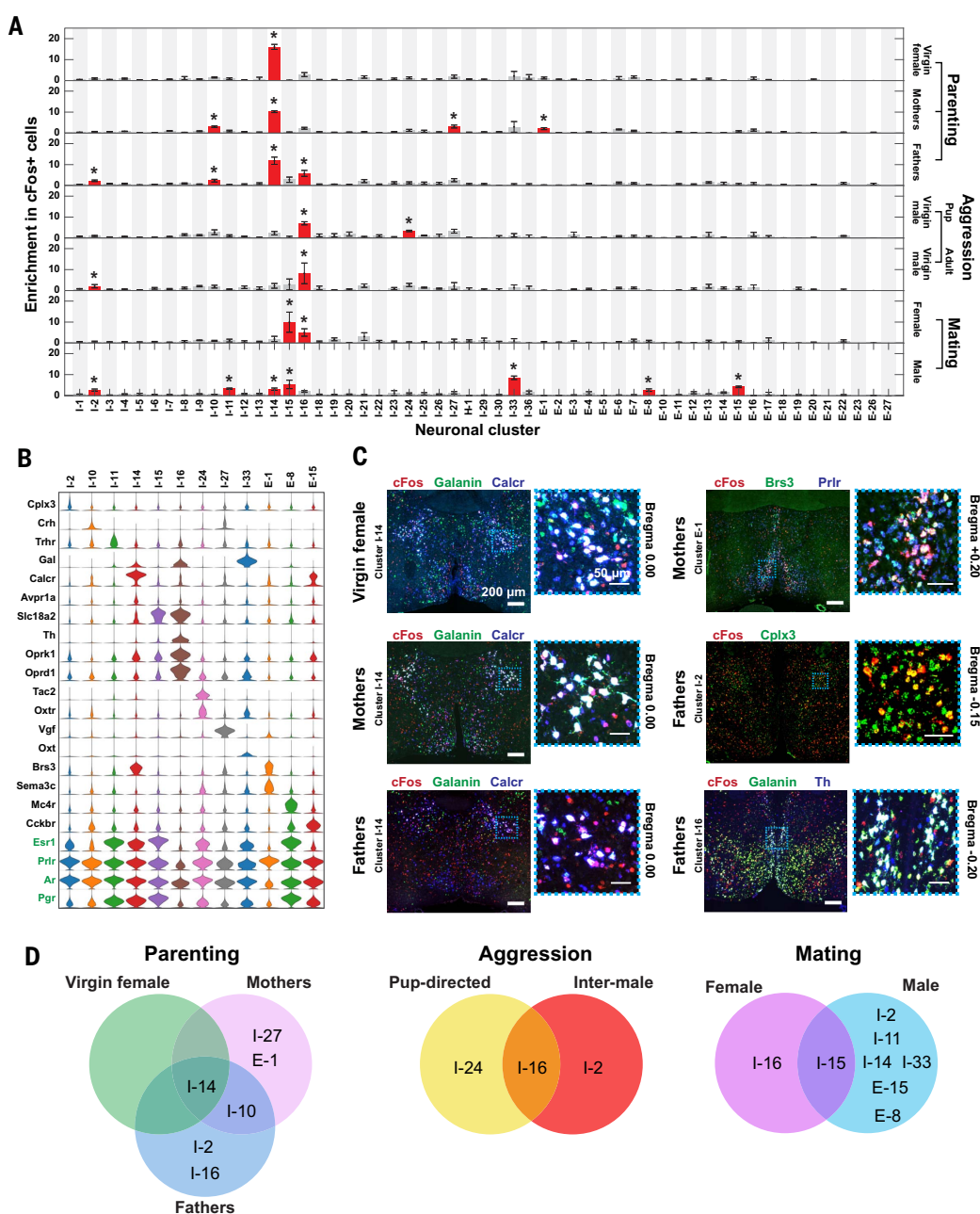
suggesting that it may contain unresolved subpopulations, which may partially mask a sexual dimorphism in SDN-POA cell populations.

We next considered clusters enriched in the expression of oxytocin receptor (Oxtr), an important modulator of social behaviors that exerts its effects broadly throughout the brain (47). Although the low expression level of Oxtr has previously made it challenging to identify oxytocin targets, the high sensitivity of MERFISH allowed us to detect enrichment of Oxtr in multiple clusters (Fig. 6, I and J). For example, the Oxtr-enriched BNST cluster I-24 coexpressed multiple sex hormone receptors as well as the neuropeptide Tac2 implicated in social isolation stress (48), aggression, and fear (48, 49), suggesting the involvement of oxytocin signaling in these functions. This clus-

ter was specifically activated after pup-directed aggression by virgin males as described below, corroborating studies that implicate the BNST in this function (50). This highlights a seemingly paradoxical role for Oxtr in agonistic pup encounters versus its known roles in affiliative behaviors (47). Oxtr was also found in the VLPO cluster I-5, implying that oxytocin might have a role in the modulation of VLPO functions such as sleep or temperature sensing (4, 51–53).

The high throughput of MERFISH measurements allowed us to identify some extremely rare cell types. GnRH-expressing cells (E-30) represent a rare cell population dispersed within the preoptic area and basal forebrain that integrates and orchestrates peripheral and central aspects of reproduction (54–56). Only a few cells were

Fig. 8. Neuronal clusters activated during specific social behaviors revealed with MERFISH. (A) Enrichment in cFos-positive cells within each neuronal cluster observed in males or females after displaying a given social behavior. Red bars marked with asterisks are clusters with statistically significant enrichment in cFos-positive cells, as compared with the fraction of cFos-positive cells in all cells (binomial test; false-discovery rate < 5%). Error bars represent standard error of the mean ($n = 3$ to 5 replicates). We measured fewer slices in behaviorally stimulated animals than in naive animals (4 versus 12 slices per animal) (29), and only clusters in which at least 10 cells are present in two or more behavior replicates are depicted. (B) Expression distributions of selected marker genes and genes of interest for neuronal clusters enriched in cFos-positive cells in the tested social behaviors. Expression distributions are calculated as in Fig. 2. (C) Representative *in situ* hybridization images of 16- μ m-thick sections from the preoptic region showing cFos expression in cells expressing markers of neuronal clusters activated during parenting, in virgin females, mothers, and fathers. Regions in blue dashed boxes are magnified and shown on the right. Red, green, and blue mark the listed genes, and white (or yellow for I-2) indicates coexpression in the merged images. Clusters that cannot be distinguished by a combination of two marker genes plus their spatial location (I-27 and I-10) were not tested. (D) Venn diagrams summarizing the clusters that were activated during specific behaviors in different sexes or physiological states.



found to express appreciable GnRH in our scRNA-seq data and did not form a distinct cluster. By contrast, MERFISH identified a GnRH-enriched cluster (Fig. 6, K and L), which expressed remarkably low levels of Esr1 and Ar (Fig. 6K), suggesting that GnRH neurons may receive indirect feedback from circulating hormones within the hypothalamic–pituitary–gonadal (HPG) axis, potentially through synaptic input from hormone-responsive cell-types such as Kisspeptin (Kiss)-expressing cells (57).

Partition of previously defined cell types into multiple cell populations

Our MERFISH data also partitioned a number of previously reported single cell types—for example,

Gal-expressing and Adcyap1-expressing neurons—into multiple distinct cell populations (Fig. 7A). We observed 10 Gal-enriched MERFISH clusters, several of which were scattered across multiple nuclei, such as cluster I-14:MPA/MPN/StHy (Fig. 7, A to C). I-14 was strongly activated during parenting, as shown below, revealing that molecularly and functionally defined cell types can spread across multiple nuclei.

Similarly, MERFISH identified 14 clusters enriched in Adcyap1 and Bdnf (Fig. 7, A, D, and E), which were previously designated as markers for warm-sensitive neurons (8). Yet only one of these clusters, E-3:AvPe/Pe/VMPO/VLPO, displayed the established spatial location of warm-sensitive cells (Fig. 7E) (8). Indeed, upon

heat stress (29), a high level of the IEG cFos was expressed in cells in the region covered by E-3, and Sncg, a marker gene of E-3's corresponding scRNA-seq cluster e13 (table S9), was highly enriched in these cFos-positive cells (Fig. 7F). E-3 expressed the leptin and prolactin receptors (Lepr and Prlr) (Fig. 7D), suggesting a mechanism by which metabolic and reproductive states may modulate thermoregulation. Preoptic cells receiving projections from Arcuate Nucleus Kiss1 cells were recently implicated in the regulation of hormonally induced hot flashes via the activation of the receptor Tacr3 (58). E-3 and e13 expressed both Kiss1 receptor and Tacr3, implicating the warm-sensitive cluster in the generation of hot flashes.

Neuronal cell types activated by key social behaviors

To investigate the role of specific neuronal populations in discrete social behaviors, we included cFos in MERFISH measurements and characterized animals after parenting, aggression, or mating. We performed clustering analysis of these behavioral samples together with naïve samples not subjected to behavioral stimuli and did not observe any cluster that was present only in behavioral samples. For each behavior, only a few neuronal clusters, each characterized by key markers, exhibited a statistically significant enrichment in cFos-positive cells (Fig. 8, A and B, and fig. S20). In addition, many other clusters showed a small fraction of cFos-positive cells, which together accounted for a substantial subset of all cFos-positive cells (Fig. 8A and fig. S20B). Activated neurons in all tested behaviors were predominantly inhibitory.

We first examined clusters preferentially activated after pup exposure, which elicits parenting behaviors in virgin females, mothers, and fathers but triggers aggression in virgin males (5, 59). We identified, with MERFISH, preferentially activated clusters—clusters enriched in cFos-positive cells (referred to as cFos enrichment hereafter) (Fig. 8, A and B, and fig. S20)—and validated, by use of two- or three-color *in situ* hybridization, all clusters that could be specifically defined by two marker genes and spatial location (Fig. 8C). In all animal groups that display parenting, I-14:MPA/MPN/StHy had substantially higher cFos enrichment than that of any other cluster (Fig. 8A and fig. S20). The expression of Gal and vasopressin receptor (Avpr1a) within this cluster (Fig. 8B) is consistent with the established role of Gal neurons in parenting (5) and their recently documented vasopressinergic input (60). Moreover, this cluster expressed a large set of hormone and peptide receptors (Fig. 8B), substantiating the complex neuromodulation of parenting (61). In addition to I-14, we observed a preferential activation of clusters by pup exposure in a state-dependent manner. In mothers and fathers, cFos enrichment was observed in Oxt-expressing cluster I-10:MPA/PaAP/SHy, and mothers additionally showed modest cFos enrichment in I-27:BNST and E-1:AvPe/Pe/MnPO/VMPO (Fig. 8 and fig. S20). Fathers additionally showed cFos enrichment in clusters I-2:BNST/StHy/MPN and in I-16:AvPe/Pe/SHy (Fig. 8 and fig. S20).

By contrast, I-14 was not preferentially activated in virgin males exposed to pups, which is consistent with their aggressive responses toward pups (5). Instead, I-16:AvPe/Pe/SHy and I-24:BNST exhibited cFos enrichment after pup-directed aggression (Fig. 8 and figs. S20 and S21). I-16 was also preferentially activated in virgin males that display inter-male aggression, as was I-2 (Fig. 8 and figs. S20 and S21), suggesting that I-16 is broadly involved in aggressive responses, whereas I-24 and I-2 may mediate differential responses to pups and adults. I-16 was also activated in fathers during parenting, which might indicate that the switch from pup-directed aggression to parenting (59, 61) occurs in circuit

nodes downstream of I-16, or that the role of I-16 in aggression is inhibited by pro-parenting circuits. The Gal- and Th-enriched cluster I-16 expressed Vmat2 (Slc18a2) and showed correspondence to the scRNA-seq cluster i16:Gal/Th (table S9), which additionally expressed Ddc, suggesting that this cell population is dopaminergic. The activation of a dopaminergic neuronal population during aggression may provide a cellular basis to understand the observations that dopamine is released during aggression and modulates aggressive behavior (6). I-16 also expressed the opioid receptors Oprd1 and Oprk1 (Fig. 8B), supporting the effects of opioid receptor ligands on aggressive encounters in mice and other rodents (62).

Next, we examined clusters activated by successful mating (29) to capture neural activity associated with appetitive and consummatory aspects of sexual behavior. The cluster I-15: AvPe/Pe/VMPO, which displayed a cell abundance enrichment in female mice compared with males (Fig. 6H), was preferentially activated in females and to a lesser extent in males after mating (Fig. 8 and figs. S20 and S21). Both I-14 and I-15—activated by parenting and mating, respectively—expressed Esr1 (Fig. 8B), which is consistent with recent findings on the involvement of Esr1-expressing cells in parenting and mating behaviors (63, 64). However, our data showed that cells activated by parenting and mating belong to two distinct cell populations localized to distinct preoptic nuclei. More generally, we found Esr1 expression in nearly all behaviorally activated clusters, suggesting that this gene alone cannot define specific behaviorally relevant cell types. In addition to I-15, which was activated in both sexes after mating, we also observed a few clusters that exhibited sexually dimorphic cFos enrichment, such as I-16 in female mating and I-2, I-11, I-14, I-33, E-8, and E-15 in male mating (Fig. 8 and figs. S20 and S21). The weak activation of the parenting cluster I-14 after male sexual behavior is consistent with our previous finding that a small subset of Gal neurons are activated in both mating and parenting (5) and may suggest a mechanism underlying the mating-dependent switch to parental behavior in virgin male mice. Intriguingly, the Th-enriched cluster I-16 was activated by different behaviors in animals of different sexes, mating in females and aggression in males, similarly to the functional sexual dimorphism observed in a recent study of AvPe Th cells (6).

Discussion

Here, we combined the power of scRNA-seq and MERFISH to create a spatially resolved and functionally aware cell atlas of the preoptic region of the mouse hypothalamus. These methods identified major cell classes and neuronal subpopulations with correlated gene expression profiles, providing cross-validations for both methods. Moreover, the two methods are complementary: scRNA-seq measured more genes than MERFISH and helped define marker genes for MERFISH, whereas MERFISH provided spatial context of

cells at high resolution as well as more accurate detection and quantification of weakly expressed genes, including functionally important genes such as neuropeptide and hormone receptors. As a result, the combined data provided a more complete picture of the transcriptional diversity and spatial organization of individual cells in the preoptic region.

We observed a remarkable diversity of neurons in this region, comprising ~70 different neuronal clusters. Transcription factors and cell-surface markers have been observed as markers of neuronal identity in the mouse spinal cord (65) and cortex (66) and the *Drosophila* olfactory system (67). In the mouse preoptic region, genes discriminating neuronal clusters were enriched for neuropeptides and molecules involved in neuromodulator synthesis and transport and for transcription factors. By contrast, neuromodulator receptors were weaker discriminators of these neuronal populations or were expressed at low levels, providing a useful note of caution in using these genes for targeted functional studies in the preoptic region. Many of these neuronal populations were defined by a combination of multiple genes, indicating that genetic intersectional approaches will be most useful in the functional interrogation of specific cell types (67).

The list of cell populations identified in this work substantially expands and further defines previously reported cell types in this region. We observed specific clusters enriched in genes previously identified as markers of functionally important preoptic cells (for example, cells involved in parenting, aggression, thermoregulation, sleep, or thirst), such as Galanin, Th, Adcyap1, Nts, Crh, Tac1, Cck, Agtr1a, Nos1, and aromatase (tables S5 and S9). Our data also resolved many of the previously described singular cell types into multiple cell populations. We observed good correlation between our data and recent scRNA-seq analyses of the whole mouse hypothalamus (68) and of the whole mouse brain (69). In the latter study, which we compared with ours in more detail because it had a larger whole hypothalamic dataset, 15 neuronal clusters were identified from ~2000 profiled hypothalamic neurons (fig. S22) (69). However, because we used ~10 times more neuronal scRNA-seq profiles to characterize about one-fifth of the whole hypothalamus (the preoptic region), we were able to analyze the preoptic region with a greater depth and thus gain finer delineation of cell populations (fig. S22B). The neuronal populations that we uncovered in the preoptic region also largely differed from cell clusters described in scRNA-seq studies of other hypothalamic areas (33, 70), perhaps suggesting a molecular and cellular distinctiveness of this brain area.

MERFISH further allowed us to map the spatial organization of cell populations. Structural features of the hypothalamus are not as visibly apparent as in laminated parts of the brain, and hypothalamic nuclei have largely been defined by subtle differences in neuronal density together with specific connectivity and functional roles (1). However, the differences versus similarities

in the cell-type composition and function of distinct nuclei in the hypothalamus remains unclear (7). MERFISH allowed us to examine the organization of distinct cell populations within individual hypothalamic nuclei, providing a framework with which to explore the molecular basis of their anatomical segregation. The spatial organizations of neuronal clusters were diverse: Many of the neuronal clusters were each primarily enriched in one or a few nuclei, whereas several clusters were substantially more dispersed. Moreover, individual nuclei were composed of multiple neuronal clusters. We also observed specific topographical organizations that can support defined modes of function; for example, the spatial proximity of aromatase- and Esr1-expressing cells may support paracrine estrogen signaling. Although aromatase- and Esr1-enriched cell populations regulate sex hormone production and signaling, rarely any of them appeared to be exclusively expressed in either sex, which is consistent with behavioral evidence that males and females are capable of exhibiting behaviors typical of the opposite sex (5, 72).

Last, the ability of MERFISH to interrogate intact tissue allowed us to include activity-dependent IEGs in our measurements, allowing the identification of neuronal populations activated by specific behaviors. Using this approach to study several social behaviors—including parenting, aggression, and mating—we observed that only a small number of neuronal clusters displayed statistically significant enrichment in cFos-positive cells after each behavior. This observation supports a model in which genetically encoded circuits composed of transcriptionally distinct neuronal types control specific hypothalamic functions. However, in all three behaviors, we also observed widespread activation of many neuronal clusters at a substantially weaker level, suggesting a secondary role for many different neuronal types in these behaviors and possibly reflecting necessary cross-talk between different behavior circuits. We caution that the large range of cFos expression levels seen in our samples suggests that some activated clusters with low levels of activity-dependent cFos induction may not have been identified if their cFos levels were below the background noise in our measurements.

This study also extended our previous work on circuits that underlie parenting behavior (5, 60) by resolving preoptic Gal neurons into several distinct subpopulations, with only one of them involved in both male and female parenting. In addition, we identified distinct cell populations that were differentially activated in mothers and fathers during parenting, providing insights into how physiological state may affect parental behavior. Moreover, we identified cell populations associated with sexual behavior in males and females as well as those involved in male aggression toward infants and conspecific males. Together, our data defined functionally relevant cell populations that underlie social behavior with a high molecular and spatial resolution.

Overall, our study demonstrates the power of combining scRNA-seq and MERFISH to map cell

types and their organization in the brain, reveal their functional roles in diverse behaviors, and generate hypotheses about structure-function relationships in neural circuits. The identification of marker gene combinations and spatial locations defining the neuronal populations in the preoptic region provides necessary tools for the precise targeting and perturbation of these neurons, thus enabling future functional studies. As an imaging-based approach, we envision that MERFISH can be combined with diverse imaging methods for anatomical tracing and functional interrogation to provide insights into how distinct cell types communicate to form functional circuits in the healthy and diseased brain, as well as in other tissues.

Methods summary

scRNA-seq of the preoptic region was performed by using protocols modified from (70) to increase neuronal survival. Tissue fixation and sectioning as well as MERFISH probe construction, staining, and imaging were performed by using established protocols (26). We imaged 155 genes in MERFISH measurements, with 135 genes imaged by using combinatorial smFISH measurements and 20 additional genes imaged by using sequential rounds of noncombinatorial FISH. The sequences of all probes used for MERFISH are provided in tables S10 and S11. Individual cells were segmented with a seeded watershed algorithm by using DAPI and total mRNA costains (29). Cell clusters were identified by using Louvain community detection on a nearest-neighbor graph built on the statistically significant principle components of gene expression (28, 31, 73) modified to allow an optimized choice of the number of nearest neighbors in the graph. Behavioral stimuli were applied to animals by using established protocols (5, 72, 74), and only animals scored as displaying the desired behavior were used for MERFISH measurements.

REFERENCES AND NOTES

- L. W. Swanson, Cerebral hemisphere regulation of motivated behavior. *Brain Res.* **886**, 113–164 (2000). doi: [10.1016/S0006-8993\(00\)02905-X](https://doi.org/10.1016/S0006-8993(00)02905-X); pmid: [1119693](https://pubmed.ncbi.nlm.nih.gov/1119693/)
- R. B. Simerly, in *The Rat Nervous System*, G. Paxinos, Ed. (Elsevier, ed. 3, 2004), pp. 335–368.
- S. M. Sternson, Hypothalamic sensory circuits: Blueprints for purposive behaviors. *Neuron* **77**, 810–824 (2013). doi: [10.1016/j.neuron.2013.02.018](https://doi.org/10.1016/j.neuron.2013.02.018); pmid: [23473313](https://pubmed.ncbi.nlm.nih.gov/23473313/)
- J. Lu et al., Selective activation of the extended ventrolateral preoptic nucleus during rapid eye movement sleep. *J. Neurosci.* **22**, 4568–4576 (2002). doi: [10.1523/JNEUROSCI.22-11-04568.2002](https://doi.org/10.1523/JNEUROSCI.22-11-04568.2002); pmid: [12040064](https://pubmed.ncbi.nlm.nih.gov/12040064/)
- Z. Wu, A. E. Autry, J. F. Bergan, M. Watabe-Uchida, C. G. Dulac, Galanin neurons in the medial preoptic area govern parental behaviour. *Nature* **509**, 325–330 (2014). doi: [10.1038/nature13307](https://doi.org/10.1038/nature13307); pmid: [24828191](https://pubmed.ncbi.nlm.nih.gov/24828191/)
- N. Scott, M. Prigge, O. Yizhar, T. Kimchi, A sexually dimorphic hypothalamic circuit controls maternal care and oxytocin secretion. *Nature* **525**, 519–522 (2015). doi: [10.1038/nature15378](https://doi.org/10.1038/nature15378); pmid: [26375004](https://pubmed.ncbi.nlm.nih.gov/26375004/)
- K. Sokolowski et al., Specification of select hypothalamic circuits and innate behaviors by the embryonic patterning gene dbx1. *Neuron* **86**, 403–416 (2015). doi: [10.1016/j.neuron.2015.03.022](https://doi.org/10.1016/j.neuron.2015.03.022); pmid: [25864637](https://pubmed.ncbi.nlm.nih.gov/25864637/)
- C. L. Tan et al., Warm-sensitive neurons that control body temperature. *Cell* **167**, 47–59.e15 (2016). doi: [10.1016/j.cell.2016.08.028](https://doi.org/10.1016/j.cell.2016.08.028); pmid: [2716062](https://pubmed.ncbi.nlm.nih.gov/2716062/)
- D. E. Leib et al., The forebrain thirst circuit drives drinking through negative reinforcement. *Neuron* **96**, 1272–1281.e4 (2017). doi: [10.1016/j.neuron.2017.11.041](https://doi.org/10.1016/j.neuron.2017.11.041); pmid: [29268095](https://pubmed.ncbi.nlm.nih.gov/29268095/)
- W. E. Allen et al., Thirst-associated preoptic neurons encode an aversive motivational drive. *Science* **357**, 1149–1155 (2017). doi: [10.1126/science.aan6747](https://doi.org/10.1126/science.aan6747); pmid: [28912243](https://pubmed.ncbi.nlm.nih.gov/28912243/)
- S. Chung et al., Identification of preoptic sleep neurons using retrograde labelling and gene profiling. *Nature* **545**, 477–481 (2017). doi: [10.1038/nature22350](https://doi.org/10.1038/nature22350); pmid: [28514446](https://pubmed.ncbi.nlm.nih.gov/28514446/)
- J. F. Poulin, B. Tasic, J. Hjerling-Leffler, J. M. Trimarchi, R. Awinaranyam, Disentangling neural cell diversity using single-cell transcriptomics. *Nat. Neurosci.* **19**, 1131–1141 (2016). doi: [10.1038/nn.4366](https://doi.org/10.1038/nn.4366); pmid: [27571192](https://pubmed.ncbi.nlm.nih.gov/27571192/)
- A. Tanay, A. Regev, Scaling single-cell genomics from phenomenology to mechanism. *Nature* **541**, 331–338 (2017). doi: [10.1038/nature21350](https://doi.org/10.1038/nature21350); pmid: [28102262](https://pubmed.ncbi.nlm.nih.gov/28102262/)
- H. Zeng, J. R. Sanes, Neuronal cell-type classification: Challenges, opportunities and the path forward. *Nat. Rev. Neurosci.* **18**, 530–546 (2017). doi: [10.1038/nrn.2017.85](https://doi.org/10.1038/nrn.2017.85); pmid: [28775344](https://pubmed.ncbi.nlm.nih.gov/28775344/)
- E. Lein, L. E. Borm, S. Linnarsson, The promise of spatial transcriptomics for neuroscience in the era of molecular cell typing. *Science* **358**, 64–69 (2017). doi: [10.1126/science.aan6827](https://doi.org/10.1126/science.aan6827); pmid: [28983044](https://pubmed.ncbi.nlm.nih.gov/28983044/)
- N. Crosetto, M. Bienko, A. van Oudenaarden, Spatially resolved transcriptomics and beyond. *Nat. Rev. Genet.* **16**, 57–66 (2015). doi: [10.1038/ng.3832](https://doi.org/10.1038/ng.3832); pmid: [25446315](https://pubmed.ncbi.nlm.nih.gov/25446315/)
- J. M. Levsky, S. M. Shenoy, R. C. Pezo, R. H. Singer, Single-cell gene expression profiling. *Science* **297**, 836–840 (2002). doi: [10.1126/science.1072241](https://doi.org/10.1126/science.1072241); pmid: [12161654](https://pubmed.ncbi.nlm.nih.gov/12161654/)
- R. Ke et al., In situ sequencing for RNA analysis in preserved tissue and cells. *Nat. Methods* **10**, 857–860 (2013). doi: [10.1038/nmeth.2563](https://doi.org/10.1038/nmeth.2563); pmid: [23852452](https://pubmed.ncbi.nlm.nih.gov/23852452/)
- J. H. Lee et al., Highly multiplexed subcellular RNA sequencing in situ. *Science* **343**, 1360–1363 (2014). doi: [10.1126/science.125012](https://doi.org/10.1126/science.125012); pmid: [24578530](https://pubmed.ncbi.nlm.nih.gov/24578530/)
- K. H. Chen, A. N. Boettiger, J. R. Moffitt, S. Wang, X. Zhuang, Spatially resolved, highly multiplexed RNA profiling in single cells. *Science* **348**, aaa6090 (2015). doi: [10.1126/science.aaa6090](https://doi.org/10.1126/science.aaa6090); pmid: [25858977](https://pubmed.ncbi.nlm.nih.gov/25858977/)
- S. Shah, E. Lubeck, W. Zhou, L. Cai, In situ transcription profiling of single cells reveals spatial organization of cells in the mouse hippocampus. *Neuron* **92**, 342–357 (2016). doi: [10.1016/j.neuron.2016.10.001](https://doi.org/10.1016/j.neuron.2016.10.001); pmid: [27764670](https://pubmed.ncbi.nlm.nih.gov/27764670/)
- X. Wang, et al., Three-dimensional intact-tissue sequencing of single-cell transcriptional states. *Science* **361**, eaat5691 (2018). doi: [10.1126/science.aat5691](https://doi.org/10.1126/science.aat5691); pmid: [29930089](https://pubmed.ncbi.nlm.nih.gov/29930089/)
- M. E. Greenberg, E. B. Ziff, L. A. Greene, Stimulation of neuronal acetylcholine receptors induces rapid gene transcription. *Science* **234**, 80–83 (1986). doi: [10.1126/science.3749894](https://doi.org/10.1126/science.3749894); pmid: [3749894](https://pubmed.ncbi.nlm.nih.gov/3749894/)
- A. M. Femino, F. S. Fay, K. Fogarty, R. H. Singer, Visualization of single RNA transcripts in situ. *Science* **280**, 585–590 (1998). doi: [10.1126/science.280.5363.585](https://doi.org/10.1126/science.280.5363.585); pmid: [9554849](https://pubmed.ncbi.nlm.nih.gov/9554849/)
- A. Raj, P. van den Bogaard, S. A. Rifkin, A. van Oudenaarden, S. Tyagi, Imaging individual mRNA molecules using multiple singly labeled probes. *Nat. Methods* **5**, 877–879 (2008). doi: [10.1038/nmeth.1253](https://doi.org/10.1038/nmeth.1253); pmid: [18806792](https://pubmed.ncbi.nlm.nih.gov/18806792/)
- J. R. Moffitt et al., High-performance multiplexed fluorescence in situ hybridization in culture and tissue with matrix imprinting and clearing. *Proc. Natl. Acad. Sci. U.S.A.* **113**, 14456–14461 (2016). doi: [10.1073/pnas.1617699113](https://doi.org/10.1073/pnas.1617699113); pmid: [27911841](https://pubmed.ncbi.nlm.nih.gov/27911841/)
- A. M. Klein et al., Droplet barcoding for single-cell transcriptomics applied to embryonic stem cells. *Cell* **161**, 1187–1201 (2015). doi: [10.1016/j.cell.2015.04.044](https://doi.org/10.1016/j.cell.2015.04.044); pmid: [26000487](https://pubmed.ncbi.nlm.nih.gov/26000487/)
- E. Z. Macosko et al., Highly parallel genome-wide expression profiling of individual cells using nanoliter droplets. *Cell* **161**, 1202–1214 (2015). doi: [10.1016/j.cell.2015.05.002](https://doi.org/10.1016/j.cell.2015.05.002); pmid: [26000488](https://pubmed.ncbi.nlm.nih.gov/26000488/)
- Materials and methods are available as supplementary materials.
- J. H. Levine et al., Data-driven phenotypic dissection of AML reveals progenitor-like cells that correlate with prognosis. *Cell* **162**, 184–197 (2015). doi: [10.1016/j.cell.2015.05.047](https://doi.org/10.1016/j.cell.2015.05.047); pmid: [26095251](https://pubmed.ncbi.nlm.nih.gov/26095251/)
- K. Shekhar et al., Comprehensive classification of retinal bipolar neurons by single-cell transcriptomics. *Cell* **166**, 1308–1323.e30 (2016). doi: [10.1016/j.cell.2016.07.054](https://doi.org/10.1016/j.cell.2016.07.054); pmid: [27565351](https://pubmed.ncbi.nlm.nih.gov/27565351/)
- S. M. Wojcik et al., A shared vesicular carrier allows synaptic corelease of GABA and glycine. *Neuron* **50**, 575–587 (2006). doi: [10.1016/j.neuron.2006.04.016](https://doi.org/10.1016/j.neuron.2006.04.016); pmid: [16701208](https://pubmed.ncbi.nlm.nih.gov/16701208/)
- R. A. Romanov et al., Molecular interrogation of hypothalamic organization reveals distinct dopaminergic neuronal subtypes. [10.1126/science.aae5324](https://doi.org/10.1126/science.aae5324)

- Nat. Neurosci.* **20**, 176–188 (2017). doi: [10.1038/nn.4462](https://doi.org/10.1038/nn.4462); pmid: [27991900](https://pubmed.ncbi.nlm.nih.gov/27991900/)
34. S. J. Shabel, C. D. Proulx, J. Piriz, R. Malinow, GABA/glutamate co-release controls habenula output and is modified by antidepressant treatment. *Science* **345**, 1494–1498 (2014). doi: [10.1126/science.1250469](https://doi.org/10.1126/science.1250469); pmid: [25237099](https://pubmed.ncbi.nlm.nih.gov/25237099/)
35. E. S. Lein *et al.*, Genome-wide atlas of gene expression in the adult mouse brain. *Nature* **445**, 168–176 (2007). doi: [10.1038/nature05453](https://doi.org/10.1038/nature05453); pmid: [17151600](https://pubmed.ncbi.nlm.nih.gov/17151600/)
36. B. Tasic *et al.*, Adult mouse cortical cell taxonomy revealed by single-cell transcriptomics. *Nat. Neurosci.* **19**, 335–346 (2016). doi: [10.1038/nn.4216](https://doi.org/10.1038/nn.4216); pmid: [26727548](https://pubmed.ncbi.nlm.nih.gov/26727548/)
37. T. Shimogori *et al.*, A genomic atlas of mouse hypothalamic development. *Nat. Neurosci.* **13**, 767–775 (2010). doi: [10.1038/nn.2545](https://doi.org/10.1038/nn.2545); pmid: [20436479](https://pubmed.ncbi.nlm.nih.gov/20436479/)
38. Z. A. Knight *et al.*, Molecular profiling of activated neurons by phosphorylated ribosome capture. *Cell* **151**, 1126–1137 (2012). doi: [10.1016/j.cell.2012.10.039](https://doi.org/10.1016/j.cell.2012.10.039); pmid: [23178128](https://pubmed.ncbi.nlm.nih.gov/23178128/)
39. R. B. Simerly, Wired for reproduction: Organization and development of sexually dimorphic circuits in the mammalian forebrain. *Annu. Rev. Neurosci.* **25**, 507–536 (2002). doi: [10.1146/annurev.neuro.25.112701.142745](https://doi.org/10.1146/annurev.neuro.25.112701.142745); pmid: [12052919](https://pubmed.ncbi.nlm.nih.gov/12052919/)
40. J. R. Moffitt *et al.*, High-throughput single-cell gene-expression profiling with multiplexed error-robust fluorescence in situ hybridization. *Proc. Natl. Acad. Sci. U.S.A.* **113**, 11046–11051 (2016). doi: [10.1073/pnas.1612826113](https://doi.org/10.1073/pnas.1612826113); pmid: [27625426](https://pubmed.ncbi.nlm.nih.gov/27625426/)
41. M. V. Wu *et al.*, Estrogen masculinizes neural pathways and sex-specific behaviors. *Cell* **139**, 61–72 (2009). doi: [10.1016/j.cell.2009.07.036](https://doi.org/10.1016/j.cell.2009.07.036); pmid: [19804754](https://pubmed.ncbi.nlm.nih.gov/19804754/)
42. X. Xu *et al.*, Modular genetic control of sexually dimorphic behaviors. *Cell* **148**, 596–607 (2012). doi: [10.1016/j.cell.2011.12.018](https://doi.org/10.1016/j.cell.2011.12.018); pmid: [22304924](https://pubmed.ncbi.nlm.nih.gov/22304924/)
43. C. Gregg *et al.*, High-resolution analysis of parent-of-origin allelic expression in the mouse brain. *Science* **329**, 643–648 (2010). doi: [10.1126/science.1190830](https://doi.org/10.1126/science.1190830); pmid: [20616232](https://pubmed.ncbi.nlm.nih.gov/20616232/)
44. T. Kudo *et al.*, Three types of neurochemical projection from the bed nucleus of the stria terminalis to the ventral tegmental area in adult mice. *J. Neurosci.* **32**, 18035–18046 (2012). doi: [10.1523/JNEUROSCI.4057-12.2012](https://doi.org/10.1523/JNEUROSCI.4057-12.2012); pmid: [23238719](https://pubmed.ncbi.nlm.nih.gov/23238719/)
45. G. Paxinos, K. Franklin, *The Mouse Brain in Stereotaxic Coordinates* (Academic Press, ed. 3, 2007).
46. Y. Tsuneyo *et al.*, Moxd1 is a marker for sexual dimorphism in the medial preoptic area, bed nucleus of the stria terminalis and medial amygdala. *Front. Neuroanat.* **11**, 26 (2017). doi: [10.3389/fnana.2017.00026](https://doi.org/10.3389/fnana.2017.00026); pmid: [28396628](https://pubmed.ncbi.nlm.nih.gov/28396628/)
47. B. J. Marlin, R. C. Froemke, Oxytocin modulation of neural circuits for social behavior. *Dev. Neurobiol.* **77**, 169–189 (2017). doi: [10.1002/dneu.22452](https://doi.org/10.1002/dneu.22452); pmid: [27626613](https://pubmed.ncbi.nlm.nih.gov/27626613/)
48. M. Zelikowsky *et al.*, The neuropeptide Tac2 controls a distributed brain state induced by chronic social isolation stress. *Cell* **173**, 1265–1279.e19 (2018). doi: [10.1016/j.cell.2018.03.037](https://doi.org/10.1016/j.cell.2018.03.037); pmid: [29775595](https://pubmed.ncbi.nlm.nih.gov/29775595/)
49. R. Andero, B. G. Dias, K. J. Resler, A role for Tac2, NkB, and Nk3 receptor in normal and dysregulated fear memory consolidation. *Neuron* **83**, 444–454 (2014). doi: [10.1016/j.neuron.2014.05.028](https://doi.org/10.1016/j.neuron.2014.05.028); pmid: [24976214](https://pubmed.ncbi.nlm.nih.gov/24976214/)
50. Y. Tsuneyo *et al.*, Functional, anatomical, and neurochemical differentiation of medial preoptic area subregions in relation to maternal behavior in the mouse. *J. Comp. Neurol.* **521**, 1633–1663 (2013). doi: [10.1002/cne.23251](https://doi.org/10.1002/cne.23251); pmid: [23124836](https://pubmed.ncbi.nlm.nih.gov/23124836/)
51. T. Gallopin *et al.*, Identification of sleep-promoting neurons in vitro. *Nature* **404**, 992–995 (2000). doi: [10.1038/35010109](https://doi.org/10.1038/35010109); pmid: [10801127](https://pubmed.ncbi.nlm.nih.gov/10801127/)
52. J. Lu, M. A. Greco, P. Shiromani, C. B. Saper, Effect of lesions of the ventrolateral preoptic nucleus on NREM and REM sleep. *J. Neurosci.* **20**, 3830–3842 (2000). doi: [10.1523/JNEUROSCI.20-10-03830.2000](https://doi.org/10.1523/JNEUROSCI.20-10-03830.2000); pmid: [10804223](https://pubmed.ncbi.nlm.nih.gov/10804223/)
53. Z. D. Zhao *et al.*, A hypothalamic circuit that controls body temperature. *Proc. Natl. Acad. Sci. U.S.A.* **114**, 2042–2047 (2017). doi: [10.1073/pnas.1616255114](https://doi.org/10.1073/pnas.1616255114); pmid: [28053227](https://pubmed.ncbi.nlm.nih.gov/28053227/)
54. C. L. Sisk, D. L. Foster, The neural basis of puberty and adolescence. *Nat. Neurosci.* **7**, 1040–1047 (2004). doi: [10.1038/nn1326](https://doi.org/10.1038/nn1326); pmid: [15452575](https://pubmed.ncbi.nlm.nih.gov/15452575/)
55. H. Yoon, L. W. Enquist, C. Dulac, Olfactory inputs to hypothalamic neurons controlling reproduction and fertility. *Cell* **123**, 669–682 (2005). doi: [10.1016/j.cell.2005.08.039](https://doi.org/10.1016/j.cell.2005.08.039); pmid: [16290037](https://pubmed.ncbi.nlm.nih.gov/16290037/)
56. U. Boehm, Z. Zou, L. B. Buck, Feedback loops link odor and pheromone signaling with reproduction. *Cell* **123**, 683–695 (2005). doi: [10.1016/j.cell.2005.09.027](https://doi.org/10.1016/j.cell.2005.09.027); pmid: [16290036](https://pubmed.ncbi.nlm.nih.gov/16290036/)
57. J. T. George, S. B. Seminara, Kisspeptin and the hypothalamic control of reproduction: Lessons from the human. *Endocrinology* **153**, 5130–5136 (2012). doi: [10.1210/en.2012-1429](https://doi.org/10.1210/en.2012-1429); pmid: [23015291](https://pubmed.ncbi.nlm.nih.gov/23015291/)
58. S. L. Padilla, C. W. Johnson, F. D. Barker, M. A. Patterson, R. D. Palmer, A neural circuit underlying the generation of hot flushes. *Cell Reports* **24**, 271–277 (2018). doi: [10.1016/j.celrep.2018.06.037](https://doi.org/10.1016/j.celrep.2018.06.037); pmid: [29996088](https://pubmed.ncbi.nlm.nih.gov/29996088/)
59. F. S. vom Saal, Time-contingent change in infanticide and parental behavior induced by ejaculation in male mice. *Physiol. Behav.* **34**, 7–15 (1985). doi: [10.1016/0031-9384\(85\)90069-1](https://doi.org/10.1016/0031-9384(85)90069-1); pmid: [4041052](https://pubmed.ncbi.nlm.nih.gov/4041052/)
60. J. Kohl *et al.*, Functional circuit architecture underlying parental behaviour. *Nature* **556**, 326–331 (2018). doi: [10.1038/s41586-018-0027-0](https://doi.org/10.1038/s41586-018-0027-0); pmid: [29643503](https://pubmed.ncbi.nlm.nih.gov/29643503/)
61. C. Dulac, L. A. O'Connell, Z. Wu, Neural control of maternal and paternal behaviors. *Science* **345**, 765–770 (2014). doi: [10.1126/science.1253291](https://doi.org/10.1126/science.1253291); pmid: [25124430](https://pubmed.ncbi.nlm.nih.gov/25124430/)
62. G. C. Teskey, M. Kavaliers, Effects of opiate agonists and antagonists on aggressive encounters and subsequent opioid-induced analgesia, activity and feeding responses in male mice. *Pharmacol. Biochem. Behav.* **31**, 43–52 (1988). doi: [10.1016/0091-9384\(88\)90069-7](https://doi.org/10.1016/0091-9384(88)90069-7); pmid: [3252259](https://pubmed.ncbi.nlm.nih.gov/3252259/)
63. Y.-Y. Fang, T. Yamaguchi, S. C. Song, N. X. Tritsch, D. Lin, A hypothalamic midbrain pathway essential for driving maternal behaviors. *Neuron* **98**, 192–207.e10 (2018). doi: [10.1016/j.neuron.2018.02.019](https://doi.org/10.1016/j.neuron.2018.02.019); pmid: [29621487](https://pubmed.ncbi.nlm.nih.gov/29621487/)
64. Y.-C. Wei *et al.*, Medial preoptic area in mice is capable of mediating sexually dimorphic behaviors regardless of gender. *Nat. Commun.* **9**, 279 (2018). doi: [10.1038/s41467-017-02648-0](https://doi.org/10.1038/s41467-017-02648-0); pmid: [29348568](https://pubmed.ncbi.nlm.nih.gov/29348568/)
65. S. Arber, Motor circuits in action: Specification, connectivity, and function. *Neuron* **74**, 975–989 (2012). doi: [10.1016/j.neuron.2012.05.011](https://doi.org/10.1016/j.neuron.2012.05.011); pmid: [22726829](https://pubmed.ncbi.nlm.nih.gov/22726829/)
66. A. Paul *et al.*, Transcriptional architecture of synaptic communication delineates GABAergic neuron identity. *Cell* **171**, 522–539.e20 (2017). doi: [10.1016/j.cell.2017.08.032](https://doi.org/10.1016/j.cell.2017.08.032); pmid: [28942923](https://pubmed.ncbi.nlm.nih.gov/28942923/)
67. H. Li *et al.*, Classifying *Drosophila* olfactory projection neuron subtypes by single-cell RNA sequencing. *Cell* **171**, 1206–1220.e22 (2017). doi: [10.1016/j.cell.2017.10.019](https://doi.org/10.1016/j.cell.2017.10.019); pmid: [29149607](https://pubmed.ncbi.nlm.nih.gov/29149607/)
68. R. Chen, X. Wu, L. Jiang, Y. Zhang, Single-cell RNA-seq reveals hypothalamic cell diversity. *Cell Reports* **18**, 3227–3241 (2017). doi: [10.1016/j.celrep.2017.03.004](https://doi.org/10.1016/j.celrep.2017.03.004); pmid: [28355573](https://pubmed.ncbi.nlm.nih.gov/28355573/)
69. A. Zeisel *et al.*, Molecular architecture of the mouse nervous system. *Cell* **174**, 999–1014.e22 (2018). doi: [10.1016/j.cell.2018.06.021](https://doi.org/10.1016/j.cell.2018.06.021); pmid: [30096314](https://pubmed.ncbi.nlm.nih.gov/30096314/)
70. J. N. Campbell *et al.*, A molecular census of arcuate hypothalamus and median eminence cell types. *Nat. Neurosci.* **20**, 484–496 (2017). doi: [10.1038/nn.4495](https://doi.org/10.1038/nn.4495); pmid: [28166221](https://pubmed.ncbi.nlm.nih.gov/28166221/)
71. S. Blackshaw *et al.*, Molecular pathways controlling development of thalamus and hypothalamus: From neural specification to circuit formation. *J. Neurosci.* **30**, 14925–14930 (2010). doi: [10.1523/JNEUROSCI.4499-10.2010](https://doi.org/10.1523/JNEUROSCI.4499-10.2010); pmid: [21068293](https://pubmed.ncbi.nlm.nih.gov/21068293/)
72. T. Kimchi, J. Xu, C. Dulac, A functional circuit underlying male sexual behaviour in the female mouse brain. *Nature* **448**, 1009–1014 (2007). doi: [10.1038/nature06089](https://doi.org/10.1038/nature06089); pmid: [17676034](https://pubmed.ncbi.nlm.nih.gov/17676034/)
73. S. Pandey, K. Shekhar, A. Regev, A. F. Schier, Comprehensive identification and spatial mapping of habenular neuronal types using single-cell RNA-seq. *Curr. Biol.* **28**, 1052–1065.e7 (2018). doi: [10.1016/j.cub.2018.02.040](https://doi.org/10.1016/j.cub.2018.02.040); pmid: [29576475](https://pubmed.ncbi.nlm.nih.gov/29576475/)
74. L. Stowers, T. E. Holy, M. Meister, C. Dulac, G. Koentges, Loss of sex discrimination and male-male aggression in mice deficient for TRP2. *Science* **295**, 1493–1500 (2002). doi: [10.1126/science.1069259](https://doi.org/10.1126/science.1069259); pmid: [11823606](https://pubmed.ncbi.nlm.nih.gov/11823606/)
75. G. Fink *et al.*, MAST: A flexible statistical framework for assessing transcriptional changes and characterizing heterogeneity in single-cell RNA sequencing data. *Genome Biol.* **16**, 278 (2015). doi: [10.1186/s13059-015-0844-5](https://doi.org/10.1186/s13059-015-0844-5); pmid: [26653891](https://pubmed.ncbi.nlm.nih.gov/26653891/)
76. J. R. Moffitt *et al.*, Data from: Molecular, spatial and functional single-cell profiling of the hypothalamic preoptic region. Dryad (2018); doi: [10.5061/dryad.8t8s248](https://doi.org/10.5061/dryad.8t8s248)

ACKNOWLEDGMENTS

We thank Y. Sigal and H. Babcock for advice on sample preparation and assistance with instrumentation and J. Fan for assistance in the gene set enrichment analysis. **Funding:** This work is in part supported by the National Institutes of Health (R01MH113094 to X.Z and C.D.; R01MH111502 to C.D., X.Z., and A.R.; and R01HD082131 to C.D.). D.B.-M. and K.S. are supported in part by the National Institutes of Health Pathway to Independence Award (K99HD092542 to D.B.-M. and K99EY028625 to K.S.). A.R. was supported by the Klarman Cell Observatory, A.R., C.D., and X.Z. are Howard Hughes Medical Institute Investigators. **Author contributions:** J.R.M., D.B.-M., C.D., and X.Z. conceived the study; J.R.M., D.B.-M., and S.W.E. performed experiments with help from J.H. and J.D.P.; J.R.M., D.B.-M., S.W.E., and E.V. analyzed data, with help from K.S. and N.D.R.; K.S. and A.R. provided some of the analysis tools; J.R.M., D.B.-M., S.W.E., E.V., C.D., and X.Z. wrote the manuscript, with input from A.R., K.S., J.D.P., N.D.R., and J.H. **Competing interests:** J.R.M. and X.Z. are inventors on patents applied for by Harvard University related to MERFISH. A.R. is a founder of Celsius Therapeutics and a SAB member of Thermo Fisher Scientific, Driver Group, and Syros Pharmaceuticals. **Data and materials availability:** scRNA-seq data are available at Gene Expression Omnibus (GEO) (GSE113576). MERFISH data are available at Dryad (76), and the analysis software is available at https://github.com/ZhuangLab/MERFISH_analysis.

SUPPLEMENTARY MATERIALS

www.sciencemag.org/content/362/6416/eauu5324/suppl/DC1
Materials and Methods
Figs. S1 to S22
Tables S1 to S11
References (77–98)

20 June 2018; accepted 21 September 2018
Published online 1 November 2018
10.1126/science.aauu5324